Supplement of Atmos. Chem. Phys., 24, 487–508, 2024
https://doi.org/10.5194/acp-24-487-2024-supplement

Atmospheric Chemistry and Physics
Open Access

Supplement of

CAMx–UNIPAR simulation of secondary organic aerosol mass formed from multiphase reactions of hydrocarbons under the Central Valley urban atmospheres of California

Yujin Jo et al.

Correspondence to: Myoseon Jang (mjang@ufl.edu)

Section S1. The model parameters used in the UNIPAR model: product distributions by using lumping species and their physicochemical parameters to predict multiphase partitioning and aerosol phase reactions.

The lumping species are based on eight volatility (10^{-8}, 10^{-6}, 10^{-5}, 10^{-4}, 10^{-3}, 10^{-2}, 10^{-1}, and 10^{-0} in mmHg) and six reactivity categories such as very fast (VF), fast (F), medium (M), slow (S), partitioning only (P), and multi-alcohol (MA). Explicit species such as glyoxal (GLY), methylglyoxal (MGLY), and isoprene epoxydiols (IEPOX) are additionally included.

The description of UNIPAR model parameters, such as molecular weight (MW_i), oxygen-to-carbon ratio ($O{:}C_i$), and hydrogen bonding (HB_i), are described in Sect. 2.1 of the main manuscript. These parameters are reported in Tables S1–S5 below.

Table S1. Averaged molecular weight (MW) (g mol^{-1}) of lumping species.

Lumped Species	Aromatic	Alkane	Terpene	Sesquiterpene	Isoprene
1VF	216.0	239.6	210.6	100.0	100.0
2VF	199.0	218.9	162.1	176.1	100.0
3VF	182.0	198.1	207.1	100.0	100.0
4VF	164.0	177.4	134.1	132.1	118.1
5VF	147.0	156.6	156.4	130.1	100.0
6VF	156.0	135.8	142.1	142.1	116.1
7VF	149.0	115.1	100.6	100.0	100.4
8VF	95.0	94.3	99.1	100.0	100.1
1F	234.0	138.3	100.0	254.9	100.0
2F	217.0	131.7	100.0	249.7	100.0
3F	199.0	125.0	100.0	245.5	100.0
4F	192.0	118.4	184.2	223.0	177.1
5F	163.0	111.7	163.5	206.1	100.0
6F	148.0	105.1	116.8	181.3	102.1
7F	128.0	98.4	114.1	100.0	121.7
8F	110.0	91.8	72.1	72.1	97.7
1M	193.0	126.6	475.1	261.9	239.3
2M	183.0	123.9	261.0	256.7	253.1
3M	172.0	121.1	216.1	246.2	189.4
4M	196.0	118.3	179.1	238.4	167.8
5M	152.0	115.6	169.4	211.3	179.1
6M	141.0	112.8	168.1	156.0	121.1
7M	131.0	110.0	127.7	92.3	137.5
8M	121.0	107.3	195.2	92.4	74.9
1S	207.0	225.3	362.1	342.5	100.0
2S	192.0	214.9	312.2	253.8	298.7
3S	176.0	203.0	219.4	232.2	224.1
4S	160.0	191.1	211.6	252.8	179.1
5S	145.0	179.3	204.4	188.4	171.1
6S	129.0	167.4	170.5	176.5	139.3
7S	113.0	155.5	236.3	163.1	100.5
8S	98.0	143.6	200.0	123.2	103.8
1P	257.0	264.7	321.2	295.4	260.7
2P	232.0	218.6	316.4	234.6	226.0
3P	208.0	207.1	265.7	328.0	165.1
4P	183.0	195.5	224.9	185.9	192.8
5P	158.0	184.0	213.5	252.3	222.1
6P	133.0	172.5	230.6	157.1	155.5
7P	109.0	160.9	100.0	111.7	114.8
8P	84.0	149.4	112.2	85.0	103.5
1MA	257.0	210.2	100.0	100.0	212.5
2MA	232.0	198.6	160.2	100.0	181.1
3MA	208.0	106.1	100.0	100.0	100.0
4MA	183.0	120.4	238.6	100.0	118.1
5MA	158.0	164.0	100.0	100.0	100.0
6MA	133.0	152.5	100.0	100.0	100.0
7MA	109.0	140.9	100.0	100.0	100.0
8MA	84.0	129.4	100.0	100.0	100.0
MGLY	72.1	72.1	72.1	72.1	72.1
GLY	58.0	58.0	58.0	58.0	58.0
IEPOX					118.1

Table S2. Averaged hydrogen bonding parameter (HB) of lumping species.

Lumped Species	Aromatic	Alkane	Terpene	Sesquiterpene	Isoprene
1VF	1.7	0.0	2.0	0.0	0.0
2VF	1.5	0.0	2.6	2.0	0.0
3VF	1.3	0.0	1.0	0.0	0.0
4VF	1.1	0.0	2.0	2.0	2.0
5VF	0.9	0.0	0.5	1.0	0.0
6VF	0.1	0.7	0.0	0.0	1.0
7VF	0.5	0.6	0.3	0.0	1.0
8VF	0.3	0.0	0.0	0.0	0.0
1F	1.7	0.0	0.0	2.0	0.0
2F	1.5	0.0	0.0	1.0	0.0
3F	1.2	0.0	0.0	0.3	0.0
4F	0.9	0.5	1.0	0.0	2.0
5F	0.7	0.3	1.0	0.0	0.0
6F	0.4	0.8	1.0	0.0	1.0
7F	0.2	0.7	0.0	0.0	1.0
8F	0.0	0.0	0.0	0.0	0.0
1M	2.0	0.0	1.5	1.7	4.0
2M	1.7	0.0	0.7	1.1	2.0
3M	1.4	0.0	1.0	1.0	3.0
4M	0.9	1.3	1.0	0.0	2.0
5M	0.9	2.0	0.4	0.3	1.0
6M	0.6	0.7	0.0	0.5	2.0
7M	0.3	1.0	0.1	1.5	1.0
8M	0.0	0.1	0.2	0.3	0.7
1S	1.8	1.4	3.3	1.4	0.0
2S	1.5	1.7	3.7	1.4	2.0
3S	1.3	0.8	1.8	1.1	2.0
4S	1.1	1.3	1.0	0.0	1.0
5S	0.9	1.0	1.1	0.6	1.7
6S	0.7	0.5	0.7	0.1	2.0
7S	0.4	0.5	1.5	0.0	1.4
8S	0.2	0.1	1.0	0.3	1.3
1P	2.2	1.5	2.9	2.1	3.3
2P	1.9	1.7	1.6	2.6	4.0
3P	1.6	0.9	2.5	0.0	3.6
4P	1.2	0.6	2.0	1.9	2.5
5P	0.9	0.7	1.3	0.0	1.0
6P	0.5	0.4	1.0	0.5	1.4
7P	0.2	0.3	0.0	1.1	2.0
8P	0.0	0.2	0.0	0.9	0.4
1MA	2.2	0.0	0.0	0.0	4.5
2MA	1.9	0.0	3.0	0.0	4.0
3MA	1.6	0.8	0.0	0.0	0.0
4MA	1.2	3.0	1.0	0.0	3.0
5MA	0.9	0.0	0.0	0.0	0.0
6MA	0.5	0.0	0.0	0.0	0.0
7MA	0.2	0.0	0.0	0.0	0.0
8MA	0.0	0.0	0.0	0.0	0.0
MGLY	0.0	0.0	0.0	0.0	0.0
GLY	0.0	0.0	0.0	0.0	0.0
IEPOX					2.0

Table S3. Averaged oxygen to carbon ratio (O:C) of lumping species.

Lumped Species	Aromatic	Alkane	Terpene	Sesquiterpene	Isoprene
1VF	0.9	0.5	0.8	0.4	0.4
2VF	0.9	0.5	1.2	1.0	0.4
3VF	0.9	0.5	1.6	0.4	0.4
4VF	0.8	0.5	1.3	0.8	1.0
5VF	0.8	0.3	0.6	0.8	0.4
6VF	0.4	0.6	0.7	0.7	1.0
7VF	0.5	0.9	0.8	0.4	0.8
8VF	0.7	0.7	0.8	0.4	0.8
1F	1.0	0.5	0.4	0.4	0.4
2F	1.0	0.5	0.4	0.3	0.4
3F	0.9	0.5	0.4	0.3	0.4
4F	0.7	0.6	0.3	0.2	1.2
5F	0.8	0.5	0.4	0.2	0.4
6F	0.4	0.7	0.6	0.2	0.8
7F	0.7	0.6	0.6	0.4	1.0
8F	0.7	0.6	0.7	0.7	0.3
1M	1.2	0.3	0.6	0.4	1.8
2M	1.1	0.3	0.7	0.3	2.0
3M	1.1	0.3	0.5	0.2	1.4
4M	1.0	0.8	0.5	0.2	1.5
5M	0.9	0.8	0.6	0.2	1.7
6M	0.8	0.9	0.2	0.4	1.1
7M	0.7	0.4	0.7	1.0	0.8
8M	0.6	0.3	0.4	0.5	0.7
1S	0.9	0.4	1.0	0.4	0.4
2S	0.9	0.4	1.1	0.3	2.4
3S	0.9	0.4	0.8	0.2	1.6
4S	0.9	0.4	0.5	0.3	1.8
5S	0.8	0.2	0.6	0.3	1.1
6S	0.8	0.5	0.2	1.0	1.2
7S	0.8	0.3	0.6	1.5	1.0
8S	0.8	0.5	0.4	0.9	0.9
1P	1.2	0.5	1.1	0.4	2.0
2P	1.1	1.1	0.8	0.3	1.6
3P	0.9	0.8	0.9	0.4	1.5
4P	0.8	0.4	0.6	0.5	1.6
5P	0.7	0.5	0.2	0.2	1.6
6P	0.5	0.6	1.5	1.2	1.8
7P	0.4	0.6	0.4	1.6	1.6
8P	0.2	1.8	1.9	2.1	2.3
1MA	1.2	0.3	0.4	0.4	1.5
2MA	1.1	0.3	0.6	0.4	1.2
3MA	0.9	0.8	0.4	0.4	0.4
4MA	0.8	0.6	0.6	0.4	0.6
5MA	0.7	0.3	0.4	0.4	0.4
6MA	0.5	0.3	0.4	0.4	0.4
7MA	0.4	0.3	0.4	0.4	0.4
8MA	0.2	0.3	0.4	0.4	0.4
MGLY	0.7	0.7	0.7	0.7	0.7
GLY	1.0	1.0	1.0	1.0	1.0
IEPOX					0.6

Table S4. Reactivity scale (R) of lumping species.

Lumped Species	Aromatic	Alkane	Terpene	Sesquiterpene	Isoprene
1VF	12.5	12.5	12.5	12.5	12.5
2VF	8.5	8.5	8.5	8.5	8.5
3VF	8.5	8.5	8.5	8.5	8.5
4VF	8.5	8.5	8.5	8.5	8.5
5VF	8.5	8.5	8.5	8.5	8.5
6VF	8.5	8.5	8.5	8.5	8.5
7VF	8.5	8.5	8.5	8.5	8.5
8VF	8.5	8.5	8.5	8.5	8.5
1F	12.5	12.5	12.5	12.5	12.5
2F	8.2	8.2	8.2	8.2	8.2
3F	8.2	8.2	8.2	8.2	8.2
4F	8.2	8.2	8.2	8.2	8.2
5F	8.2	8.2	8.2	8.2	8.2
6F	8.2	8.2	8.2	8.2	8.2
7F	8.2	8.2	8.2	8.2	8.2
8F	8.2	8.2	8.2	8.2	8.2
1M	12.5	12.5	12.5	12.5	12.5
2M	4.0	4.0	4.0	4.0	4.0
3M	4.0	4.0	4.0	4.0	4.0
4M	4.0	4.0	4.0	4.0	4.0
5M	4.0	4.0	4.0	4.0	4.0
6M	4.0	4.0	4.0	4.0	4.0
7M	4.0	4.0	4.0	4.0	4.0
8M	4.0	4.0	4.0	4.0	4.0
1S	12.5	12.5	12.5	12.5	12.5
2S	1.0	1.0	1.0	1.0	1.0
3S	1.0	1.0	1.0	1.0	1.0
4S	1.0	1.0	1.0	1.0	1.0
5S	1.0	1.0	1.0	1.0	1.0
6S	1.0	1.0	1.0	1.0	1.0
7S	1.0	1.0	1.0	1.0	1.0
8S	1.0	1.0	1.0	1.0	1.0
1P	12.5	12.5	12.5	12.5	12.5
2P	0.0	0.0	0.0	0.0	0.0
3P	0.0	0.0	0.0	0.0	0.0
4P	0.0	0.0	0.0	0.0	0.0
5P	0.0	0.0	0.0	0.0	0.0
6P	0.0	0.0	0.0	0.0	0.0
7P	0.0	0.0	0.0	0.0	0.0
8P	0.0	0.0	0.0	0.0	0.0
1MA	12.5	12.5	12.5	12.5	12.5
2MA	0.0	0.0	0.0	0.0	0.0
3MA	0.0	0.0	0.0	0.0	0.0
4MA	0.0	0.0	0.0	0.0	0.0
5MA	0.0	0.0	0.0	0.0	0.0
6MA	0.0	0.0	0.0	0.0	0.0
7MA	0.0	0.0	0.0	0.0	0.0
8MA	0.0	0.0	0.0	0.0	0.0
MGLY	9.0	9.0	9.0	9.0	9.0
GLY	12.5	12.5	12.5	12.5	12.5
IEPOX					2.0

Table S5. The basicity constant (pK_{BH}) of lumping species.

Lumped Species	Aromatic	Alkane	Terpene	Sesquiterpene	Isoprene
1VF	-1.5	-1.5	-1.5	-1.5	-1.5
2VF	-1.5	-1.5	-1.5	-1.5	-1.5
3VF	-1.5	-1.5	-1.5	-1.5	-1.5
4VF	-1.5	-1.5	-1.5	-1.5	-1.5
5VF	-1.5	-1.5	-1.5	-1.5	-1.5
6VF	-1.5	-1.5	-1.5	-1.5	-1.5
7VF	-1.5	-1.5	-1.5	-1.5	-1.5
8VF	-1.5	-1.5	-1.5	-1.5	-1.5
1F	-1.5	-1.5	-1.5	-1.5	-1.5
2F	-1.5	-1.5	-1.5	-1.5	-1.5
3F	-1.5	-1.5	-1.5	-1.5	-1.5
4F	-1.5	-1.5	-1.5	-1.5	-1.5
5F	-1.5	-1.5	-1.5	-1.5	-1.5
6F	-1.5	-1.5	-1.5	-1.5	-1.5
7F	-1.5	-1.5	-1.5	-1.5	-1.5
8F	-1.5	-1.5	-1.5	-1.5	-1.5
1M	-1.5	-1.5	-1.5	-1.5	-1.5
2M	-1.5	-1.5	-1.5	-1.5	-1.5
3M	-1.5	-1.5	-1.5	-1.5	-1.5
4M	-1.5	-1.5	-1.5	-1.5	-1.5
5M	-1.5	-1.5	-1.5	-1.5	-1.5
6M	-1.5	-1.5	-1.5	-1.5	-1.5
7M	-1.5	-1.5	-1.5	-1.5	-1.5
8M	-1.5	-1.5	-1.5	-1.5	-1.5
1S	-2.0	-2.0	-2.0	-2.0	-2.0
2S	-2.0	-2.0	-2.0	-2.0	-2.0
3S	-2.0	-2.0	-2.0	-2.0	-2.0
4S	-2.0	-2.0	-2.0	-2.0	-2.0
5S	-2.0	-2.0	-2.0	-2.0	-2.0
6S	-2.0	-2.0	-2.0	-2.0	-2.0
7S	-2.0	-2.0	-2.0	-2.0	-2.0
8S	-2.0	-2.0	-2.0	-2.0	-2.0
1P	-2.0	-2.0	-2.0	-2.0	-2.0
2P	0.0	0.0	0.0	0.0	0.0
3P	0.0	0.0	0.0	0.0	0.0
4P	0.0	0.0	0.0	0.0	0.0
5P	0.0	0.0	0.0	0.0	0.0
6P	0.0	0.0	0.0	0.0	0.0
7P	0.0	0.0	0.0	0.0	0.0
8P	0.0	0.0	0.0	0.0	0.0
1MA	-2.0	-2.0	-2.0	-2.0	-2.0
2MA	0.0	0.0	0.0	0.0	0.0
3MA	0.0	0.0	0.0	0.0	0.0
4MA	0.0	0.0	0.0	0.0	0.0
5MA	0.0	0.0	0.0	0.0	0.0
6MA	0.0	0.0	0.0	0.0	0.0
7MA	0.0	0.0	0.0	0.0	0.0
8MA	0.0	0.0	0.0	0.0	0.0
MGLY	-1.5	-1.5	-1.5	-1.5	-1.5
GLY	-1.5	-1.5	-1.5	-1.5	-1.5
IEPOX					-1.5

Section S2. Summary of the configuration of the regional model

Table S6. Model configurations

WRF v4.1 configuration	
Horizontal resolution	D01(36 × 36km), D02(12 × 12km), D03(4 × 4km)
Microphysics	Morrison 2-moment (Morrison et al., 2009)
Longwave radiation	RRTMG (Iacono et al., 2008)
Shortwave radiation option	RRTMG (Iacono et al., 2008)
Surface-layer	Revised MM5 (Jiménez et al., 2012)
Land-surface	Pleim-Xu (Pleim and Gilliam, 2009)
Boundary-layer	ACM2 (Pleim, 2007)
Cumulus	Kain–Fritsch Cumulus Potential Scheme (D01, D02) (Berg et al., 2013)
CAMx v7.1 configuration	
Horizontal resolution	4km x 4km (185 × 185 grids)
Vertical resolution	22 eta levels
Horizontal advection	Piecewise Parabolic Method (PPM) (Colella and Woodward, 1984)
Gas-phase chemical mechanism	SAPRC07TC (Hutzell et al., 2012)
Aerosol treatment	Static 2-mode (Coarse-Fine; CF Scheme) for size distribution
Inorganic PM chemistry	ISOPPOPIA (Nenes et al., 1998; Fountoukis and Nenes, 2007)
Organic PM chemistry	UNIPAR
Dry deposition model	Resistance model (Zhang et al., 2003)
Wet deposition	Scavenging model (Seinfeld and Pandis, 1998)

Section S3. Meteorological variables (temperature, humidity, winds, Planetary Boundary Layer (PBL)), Efflorescent RH (ERH), and Deliquescence RH (DRH) and equations of statistical analyses between observations and simulations

Table S7. Statistics summary of surface temperature, relative humidity, and wind speed from WRF simulation.

		Mean (OBS)	Mean (WRF)	R	IOA	MB
San Jose	Temp. (°C)	12.42	12.07	0.93	0.96	-0.35
	RH (%)	69.16	73.32	0.87	0.92	4.17
	WS (m/s)	2.38	1.92	0.74	0.79	-0.46
Sacramento	Temp. (°C)	10.06	10.76	0.92	0.95	0.7
	RH (%)	79.27	75.64	0.91	0.95	-3.63
	WS (m/s)	1.25	1.97	0.68	0.76	0.72
Fresno	Temp. (°C)	11.04	11.41	0.93	0.96	0.37
	RH (%)	70.6	76.02	0.89	0.93	5.42
	WS (m/s)	1.07	1.63	0.61	0.71	0.55
Bakersfield	Temp. (°C)	11.52	12.65	0.92	0.94	1.13
	RH (%)	67.44	71.46	0.81	0.89	4.02
	WS (m/s)	0.94	1.63	0.53	0.63	0.69

Table S8. Statistical measures for model performance evaluation discussed in this paper.

Statistic/abbreviation	Formula	Description
Correlation Coefficient (R)	$\frac{\sum_{i=1}^{n}(M_i - \overline{M})(O_i - \overline{O})}{\sqrt{\sum_{i=1}^{n}(M_i - \overline{M})^2}\sqrt{\sum_{i=1}^{n}(O_i - \overline{O})^2}}$	- Unitless, −1 ≤ R ≤ +1 - R = 1 is perfect correlation - R = 0 is totally uncorrelated
Index Of Agreement (IOA)	$1 - \left[\frac{\sum_{i=1}^{n}(O_i - M_i)^2}{\sum_{i=1}^{n}(\lvert M_i - \overline{O}\rvert + \lvert O_i - \overline{O}\rvert)^2}\right]$	- Unitless, 0 ≤ IOA ≤ 1 (Willmott, 1984) - IOA value closer to 1 indicates better prediction
Mean Bias (MB)	$\frac{\sum_{i=1}^{n}(M_i - O_i)}{n}$	- Concentration units
Root Mean Square Error (RMSE)	$\sqrt{\frac{\sum_{i=1}^{n}(M_i - O_i)^2}{n}}$	- Concentration units
Normalized Mean Bias (NMB)	$\frac{\sum_{i=1}^{n}(M_i - O_i)}{\sum_{i=1}^{n} O_i} \times 100(\%)$	- −100% ≤ NMB ≤ +∞

Where;

n = Total number of data

M_i = Predicted values

$\overline{M}$ = Mean of the predicted values

O_i = Observed values

$\overline{O}$ = Mean of the observed values

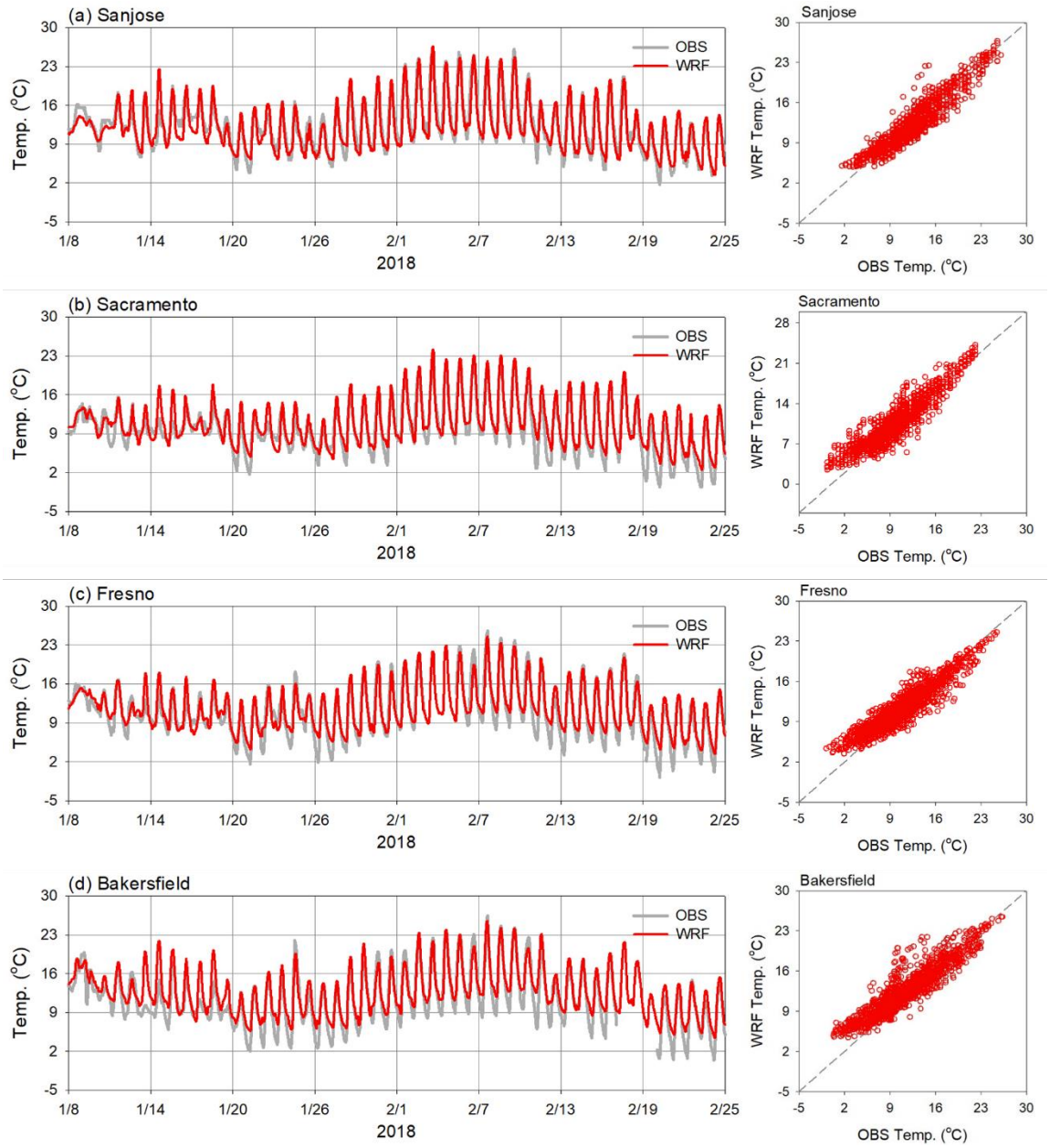

Fig. S1. Time series and scatter plots of hourly observed and simulated surface temperature at each site between January and February in 2018.

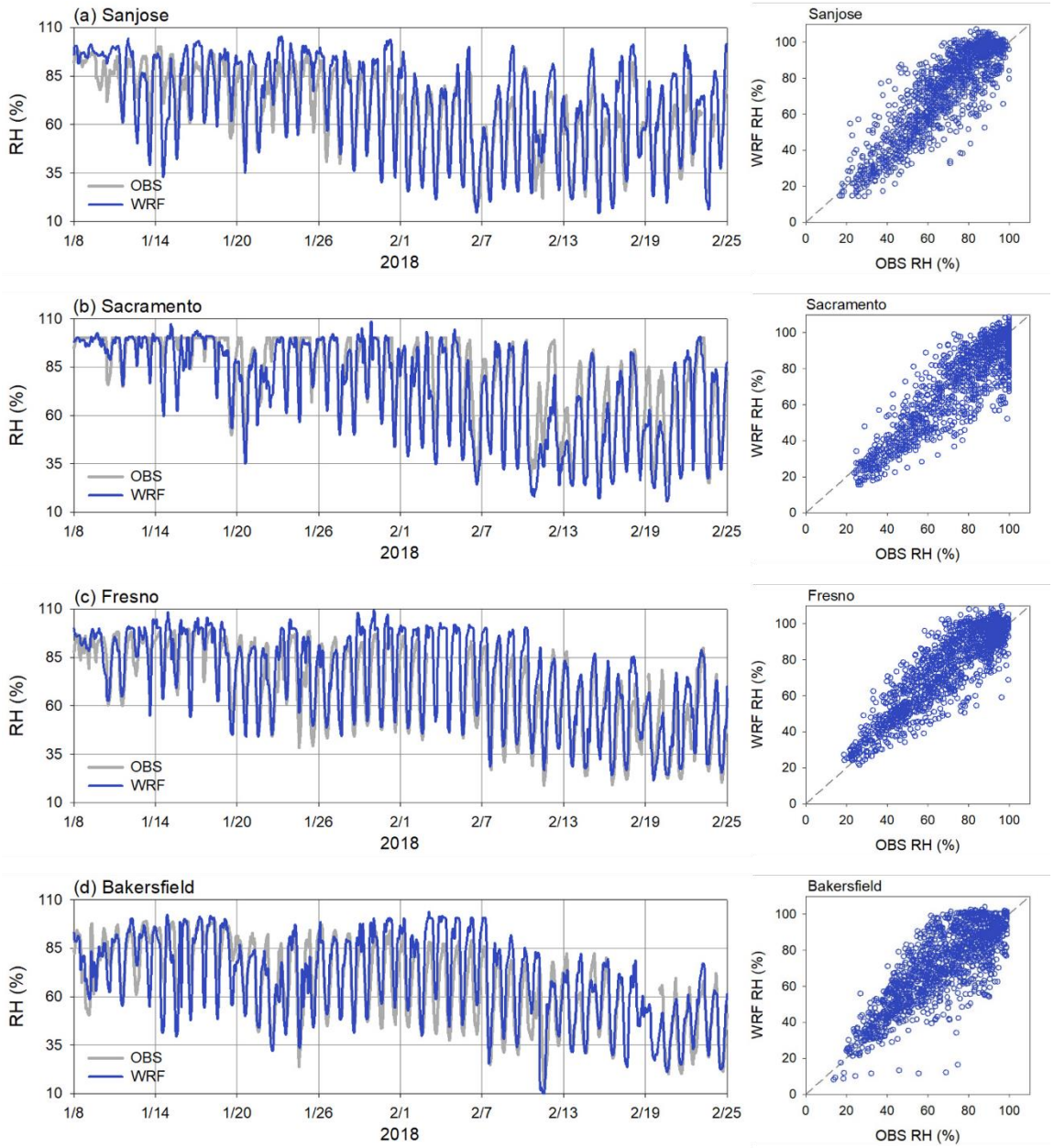

Fig. S2. Time series and scatter plots of hourly observed and simulated surface relative humidity at each site between January and February in 2018.

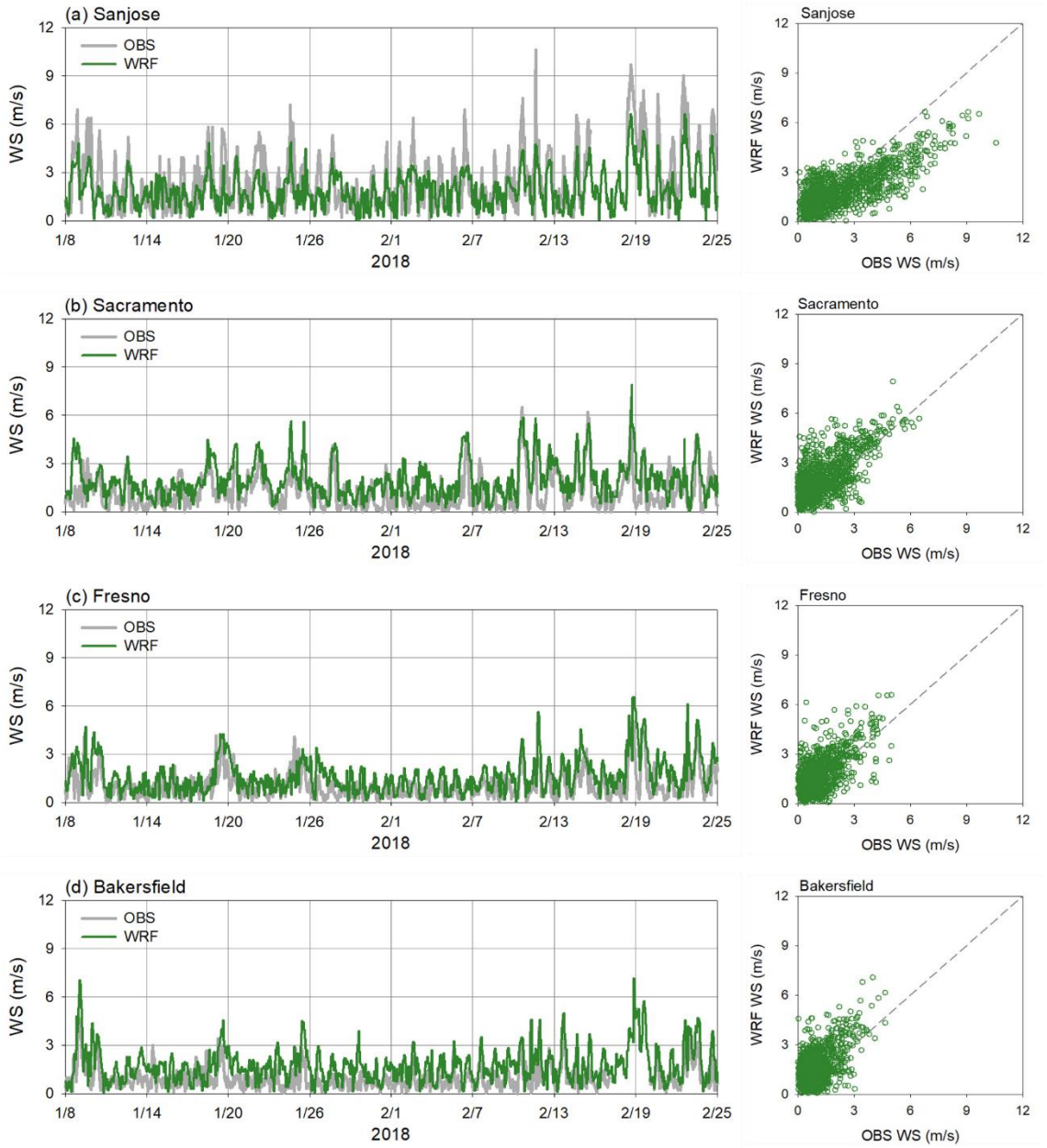

Fig. S3. Time series and scatter plots of hourly observed and simulated surface wind speed at each site between January and February in 2018.

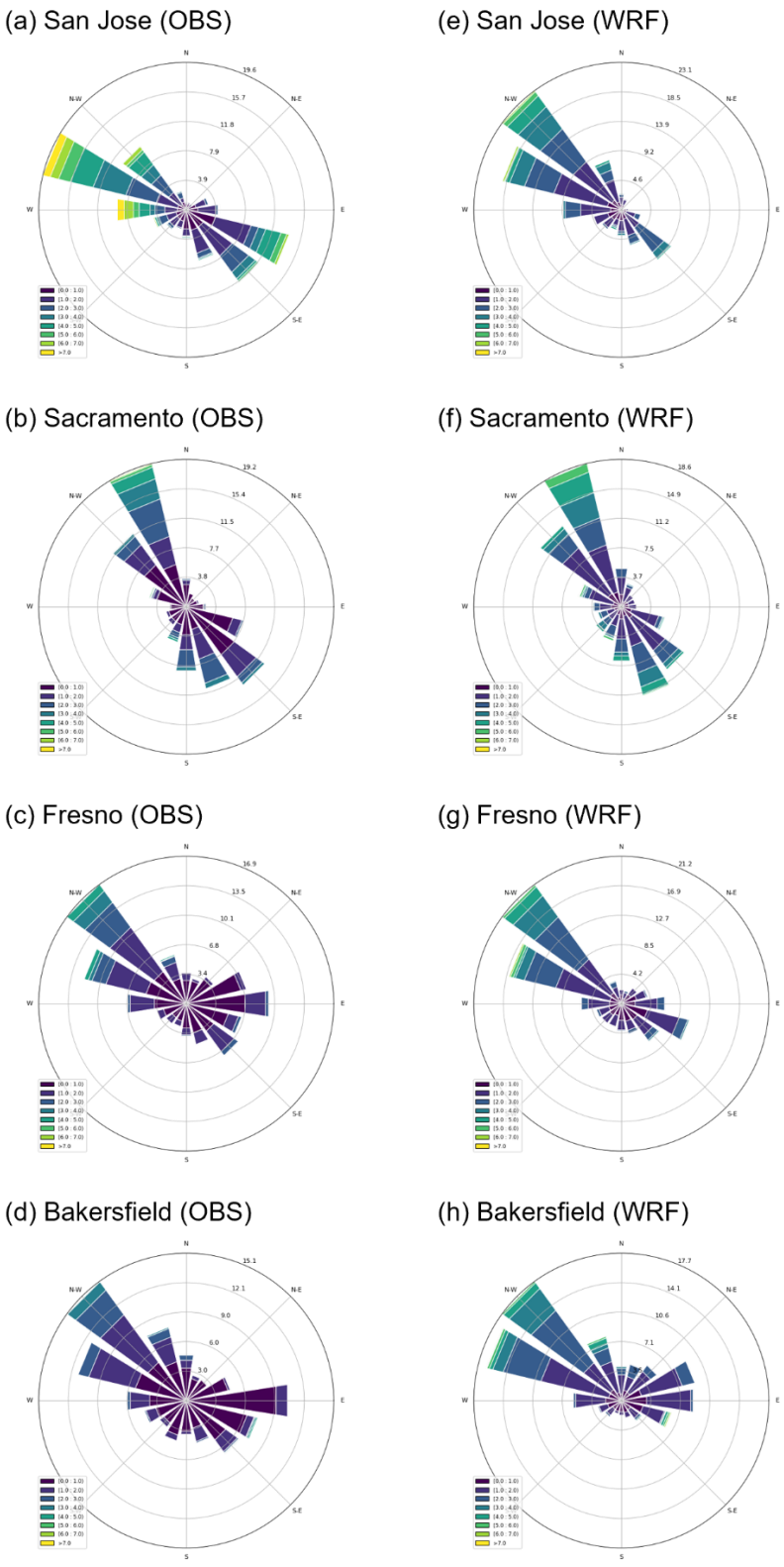

Fig. S4. Windrose plots of (a–d) observed and (e–h) simulated wind at each site between January and February in 2018.

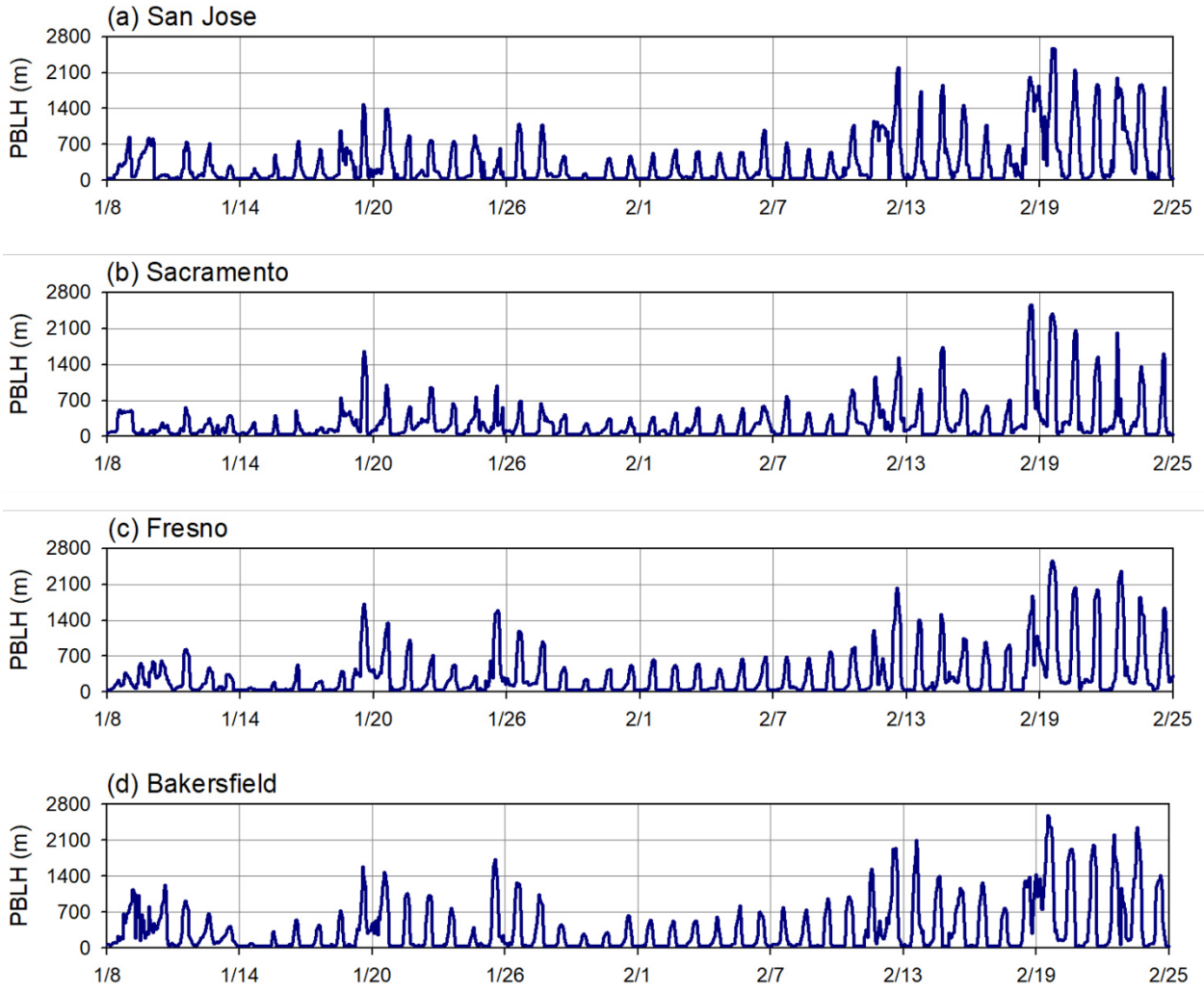

Fig. S5. Time series of hourly simulated PBL height at each site between January and February in 2018.

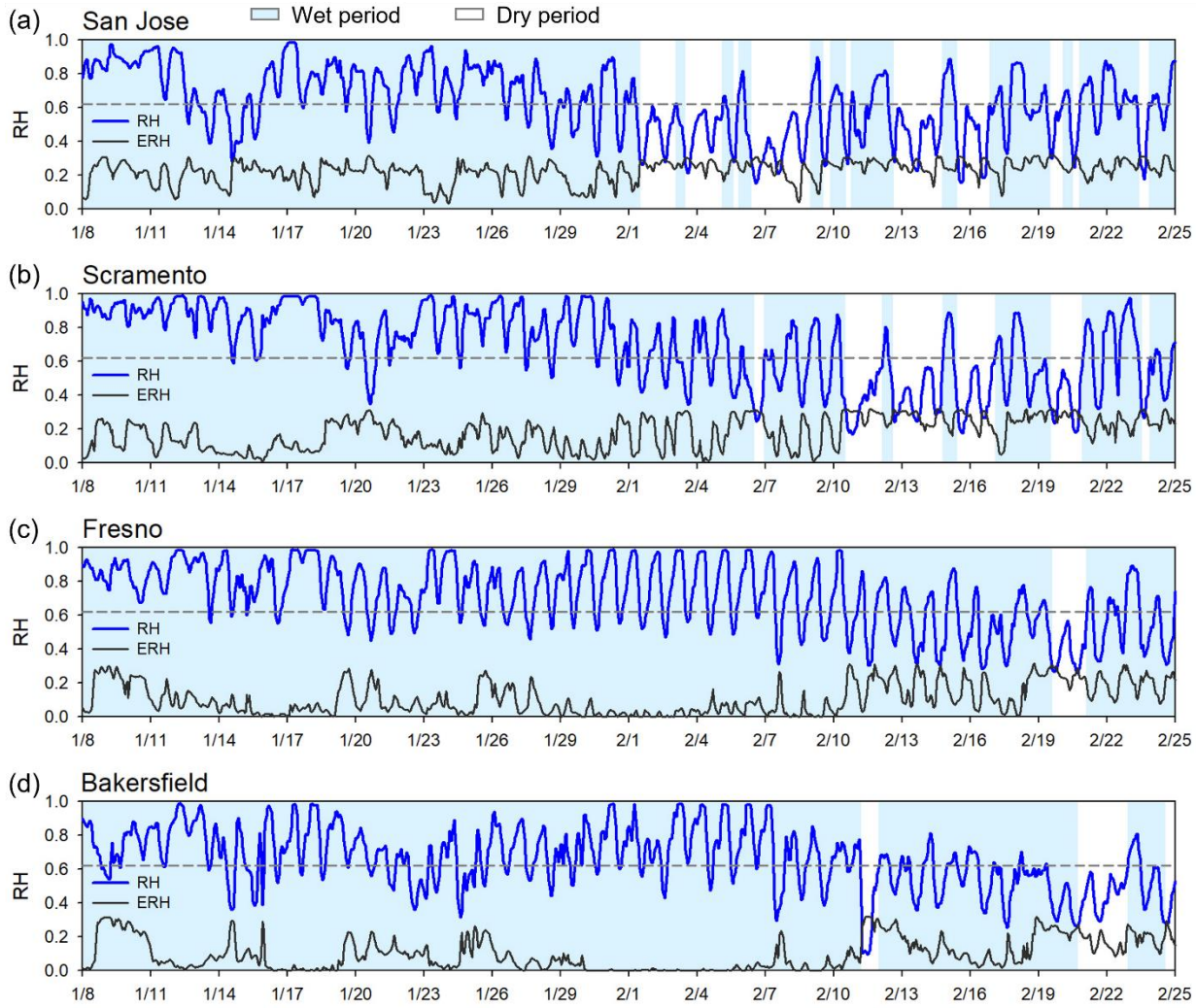

Fig. S6. Time series of hourly simulated RH and ERH. The dry and wet periods are determined by comparing RH with ERH and DRH. Anion is dominated by nitrate and DRH is almost constant nearly at 0.62.

Section S4. Time series and spatial distributions of the predicted concentrations of gas species (ozone, nitrate radicals, and SOA precursor hydrocarbons), time series of emissions of SOA precursor hydrocarbons, and time series of SOA species in the UNIPAR model.

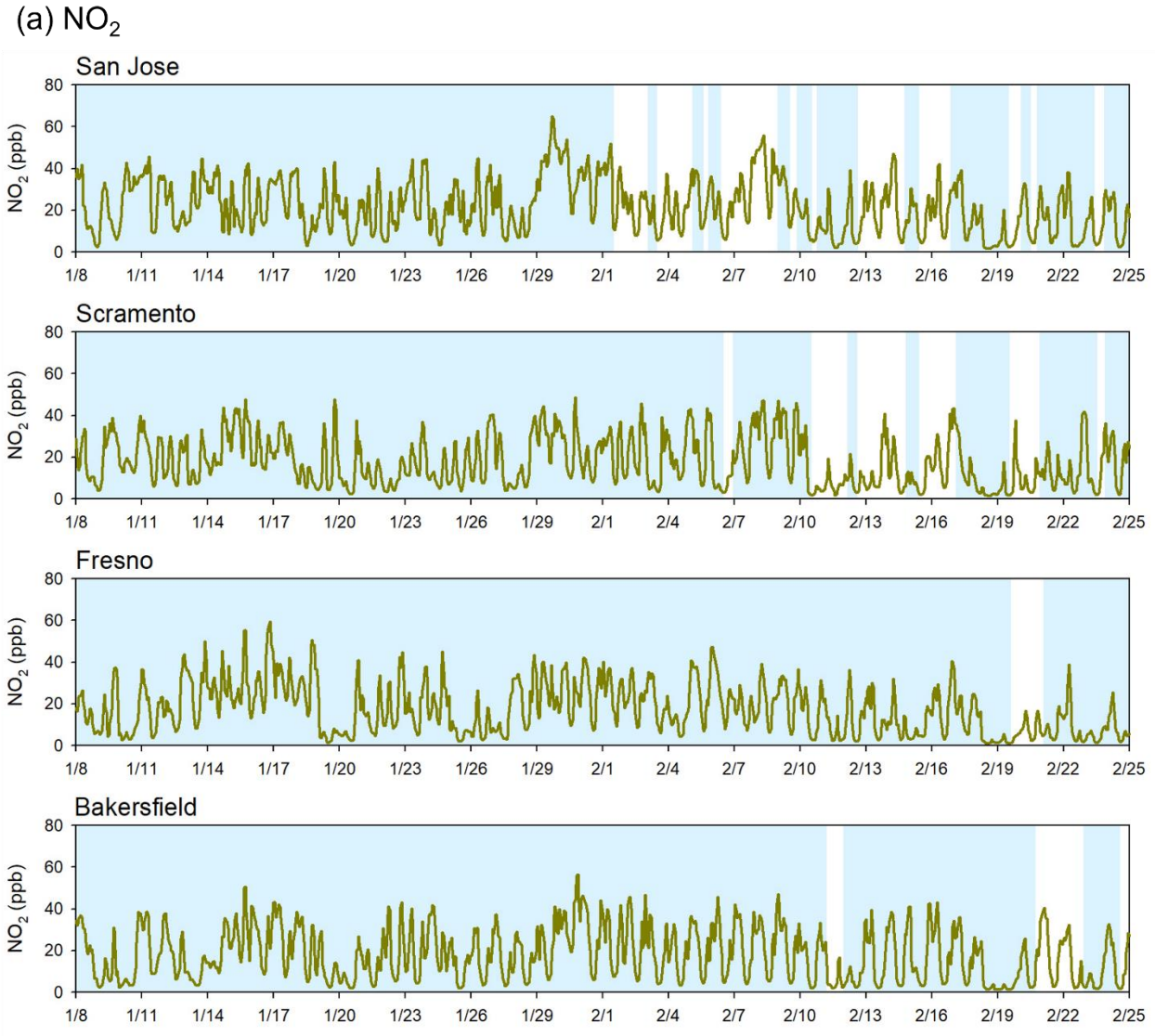

Fig. S7. Time series of hourly simulated (a) NO_2, (b) O_3, and (c) nitrate radicals at each site between January and February in 2018.

(b) O_3

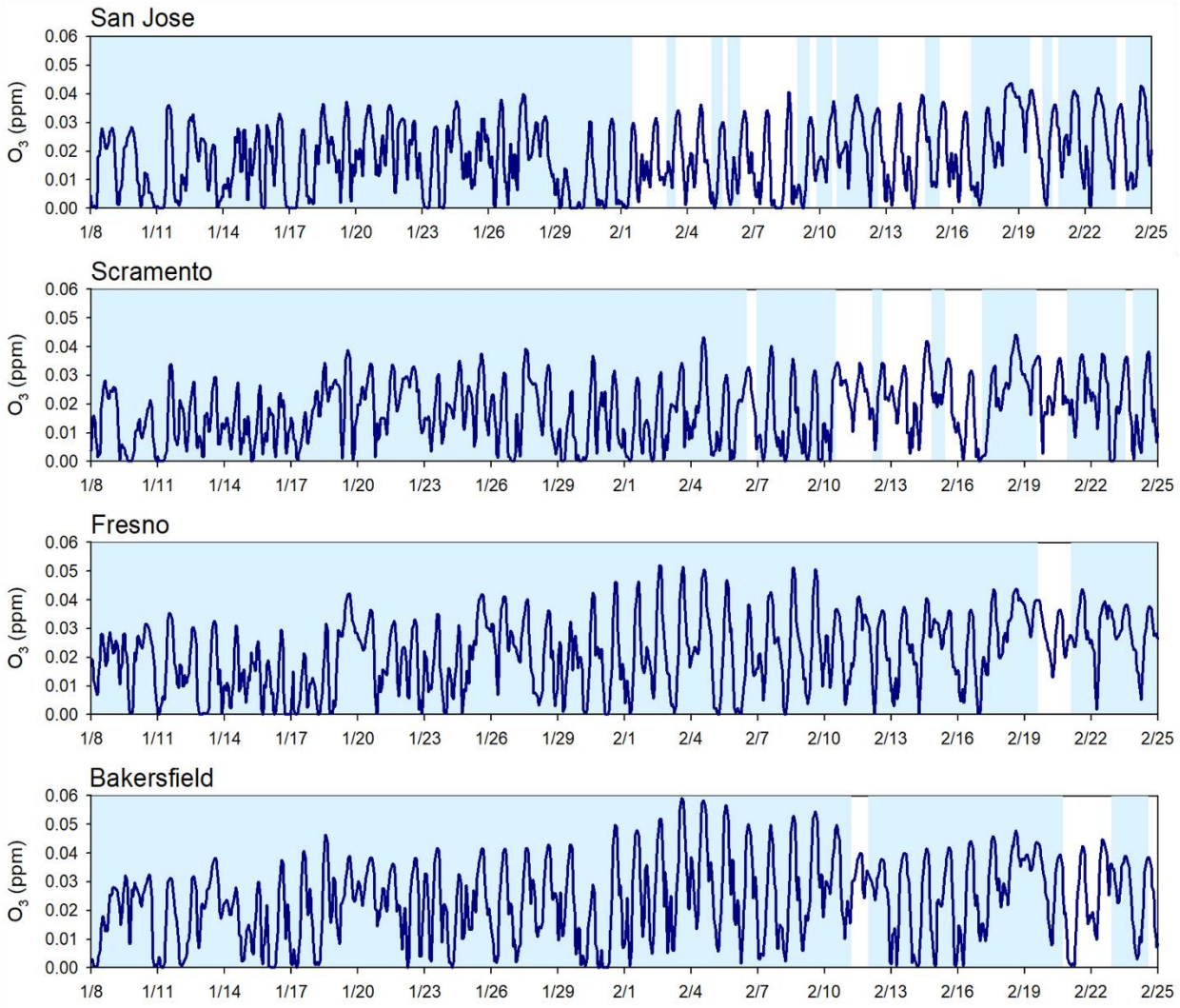

Fig. S7. (Continued)

(c) NO_3

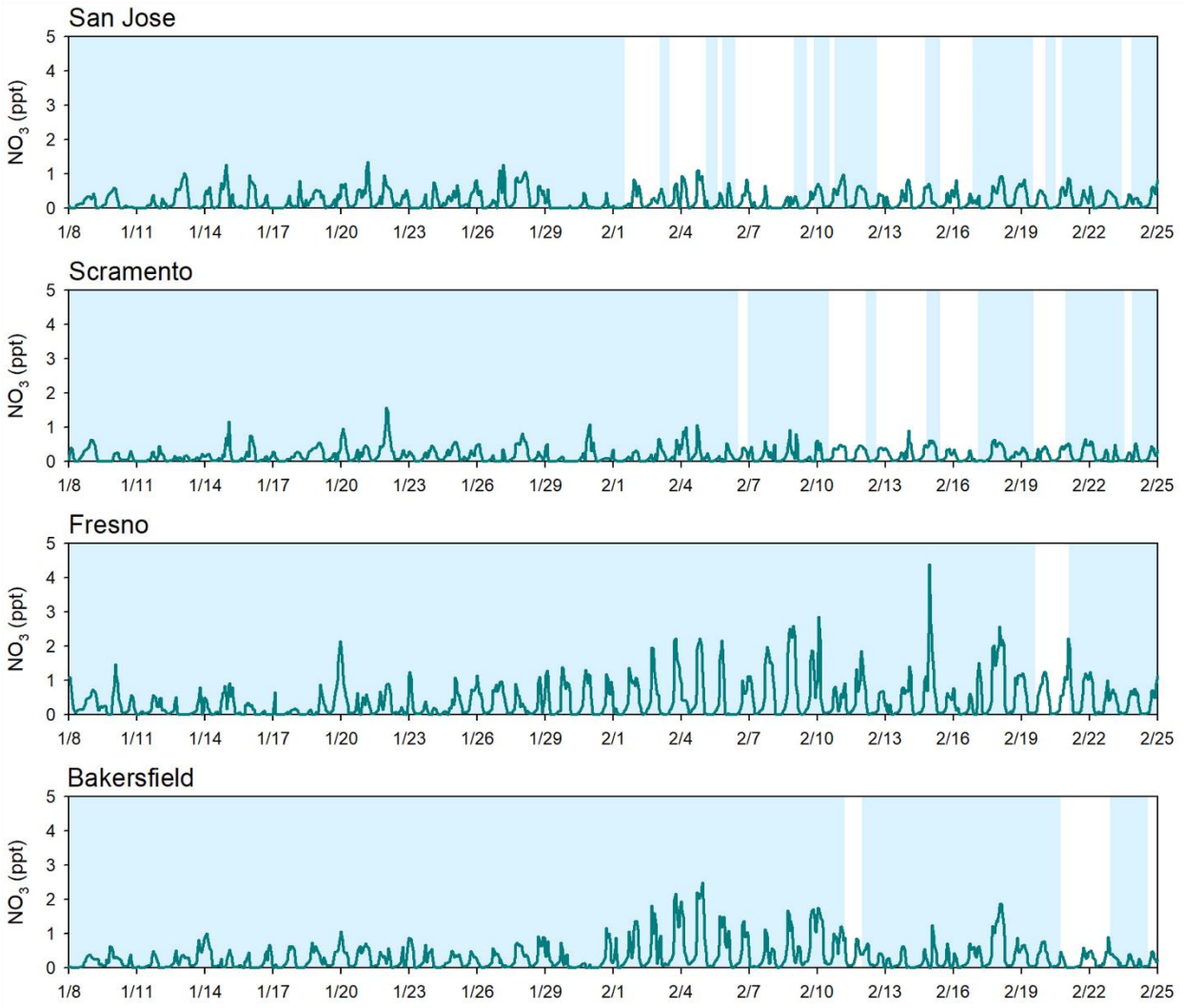

Fig. S7. (Continued)

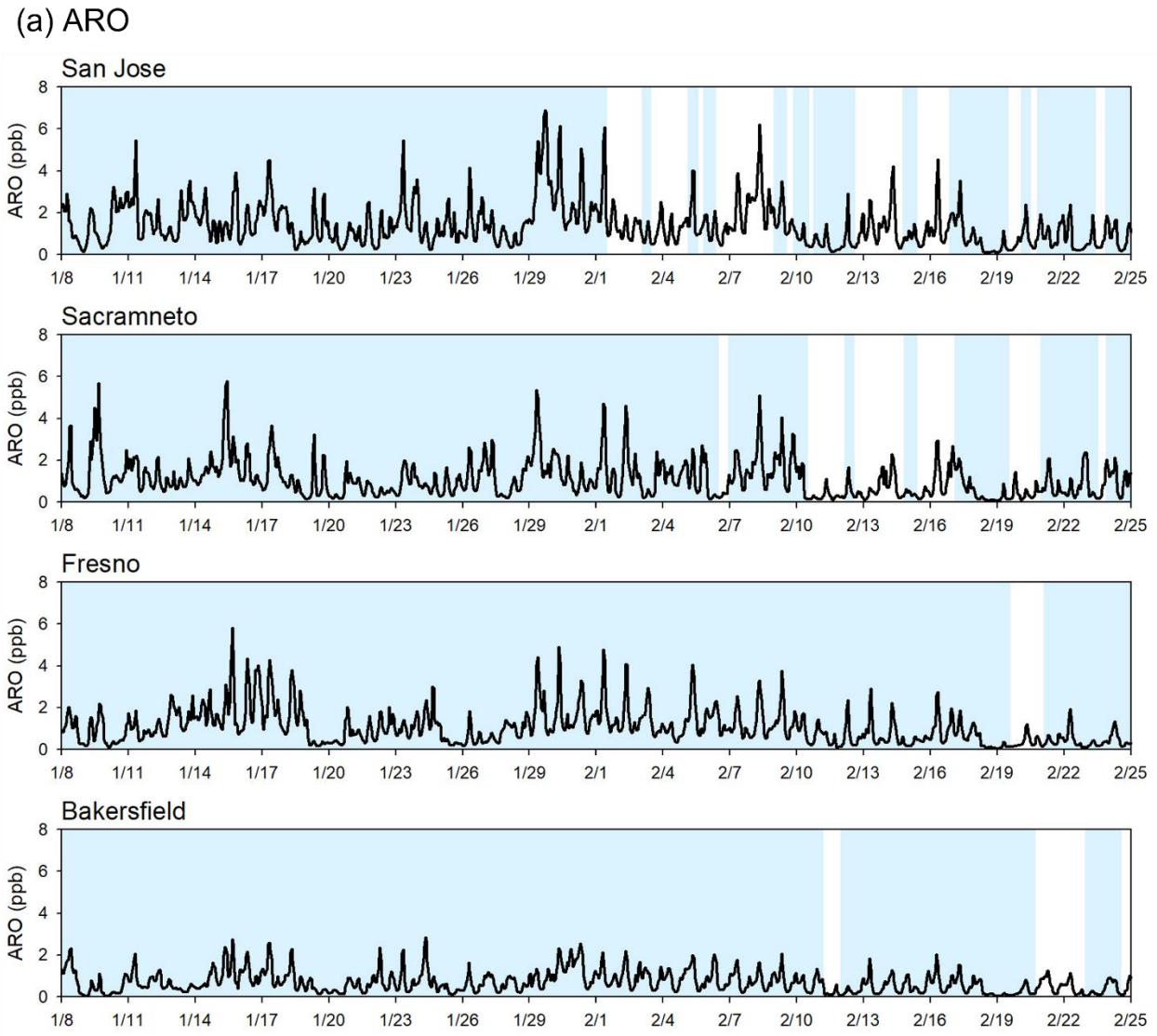

Fig. S8. Time series of hourly simulated SOA precursor hydrocarbons, (a) ARO, (b) ALK5, (c) TERP, (d) SESQ, and (e) ISOP at each site between January and February in 2018. ARO is the sum of benzene, toluene, o-xylene, p-xylene, m-xylene, and 1,2,4-trimethylbenzene.

(b) ALK5

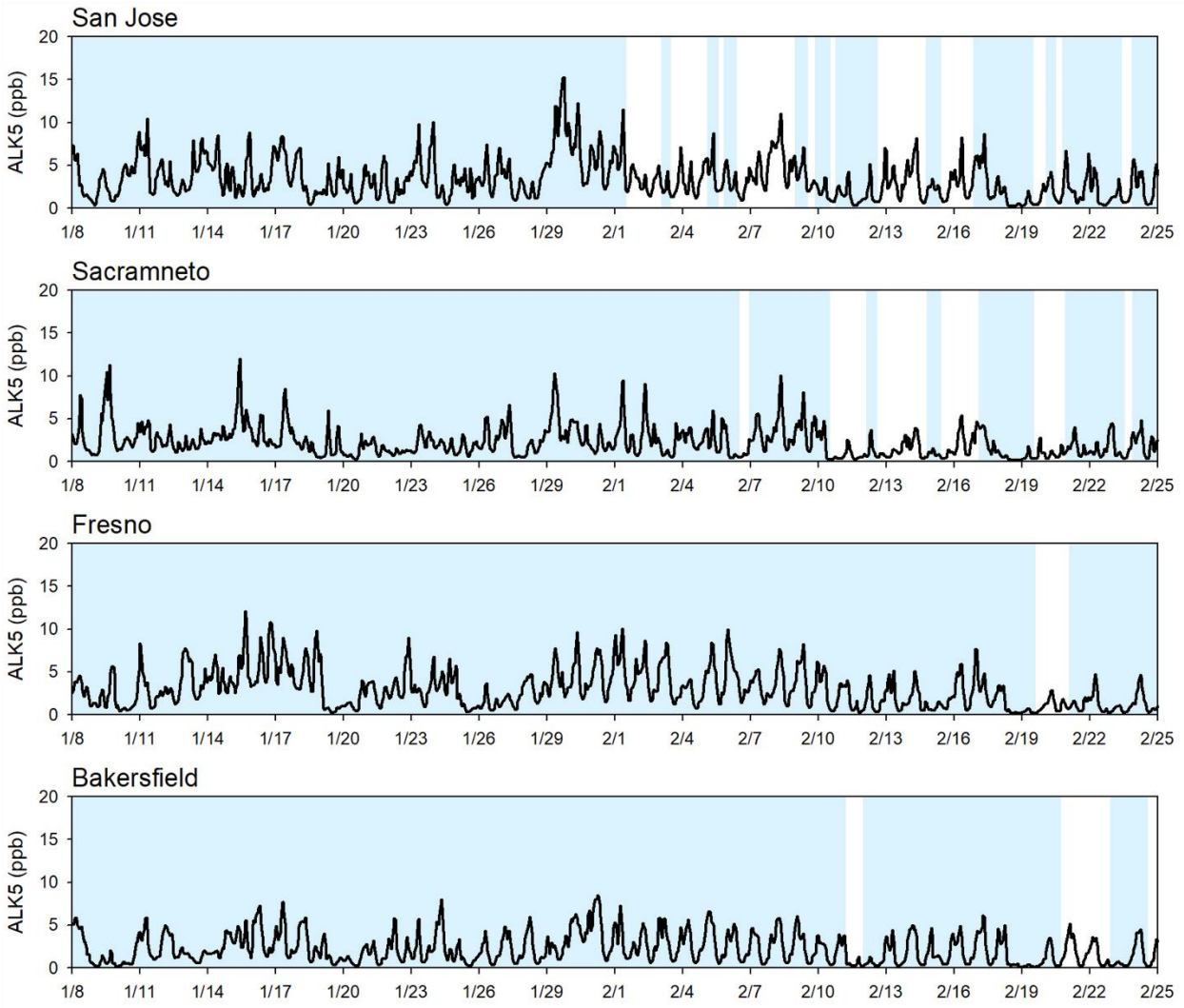

Fig. S8. (Continued)

(c) TERP

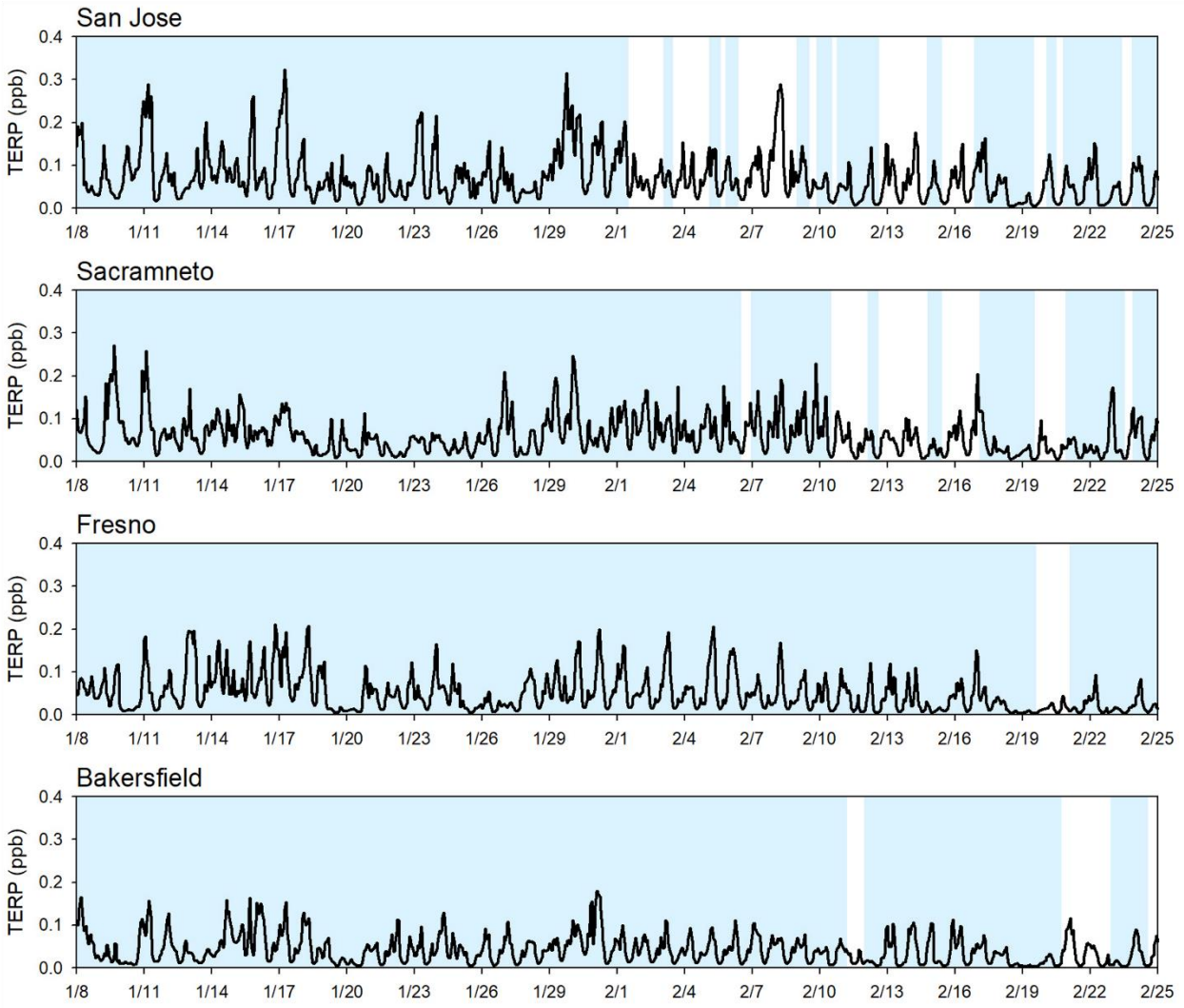

Fig. S8. (Continued)

(d) SESQ

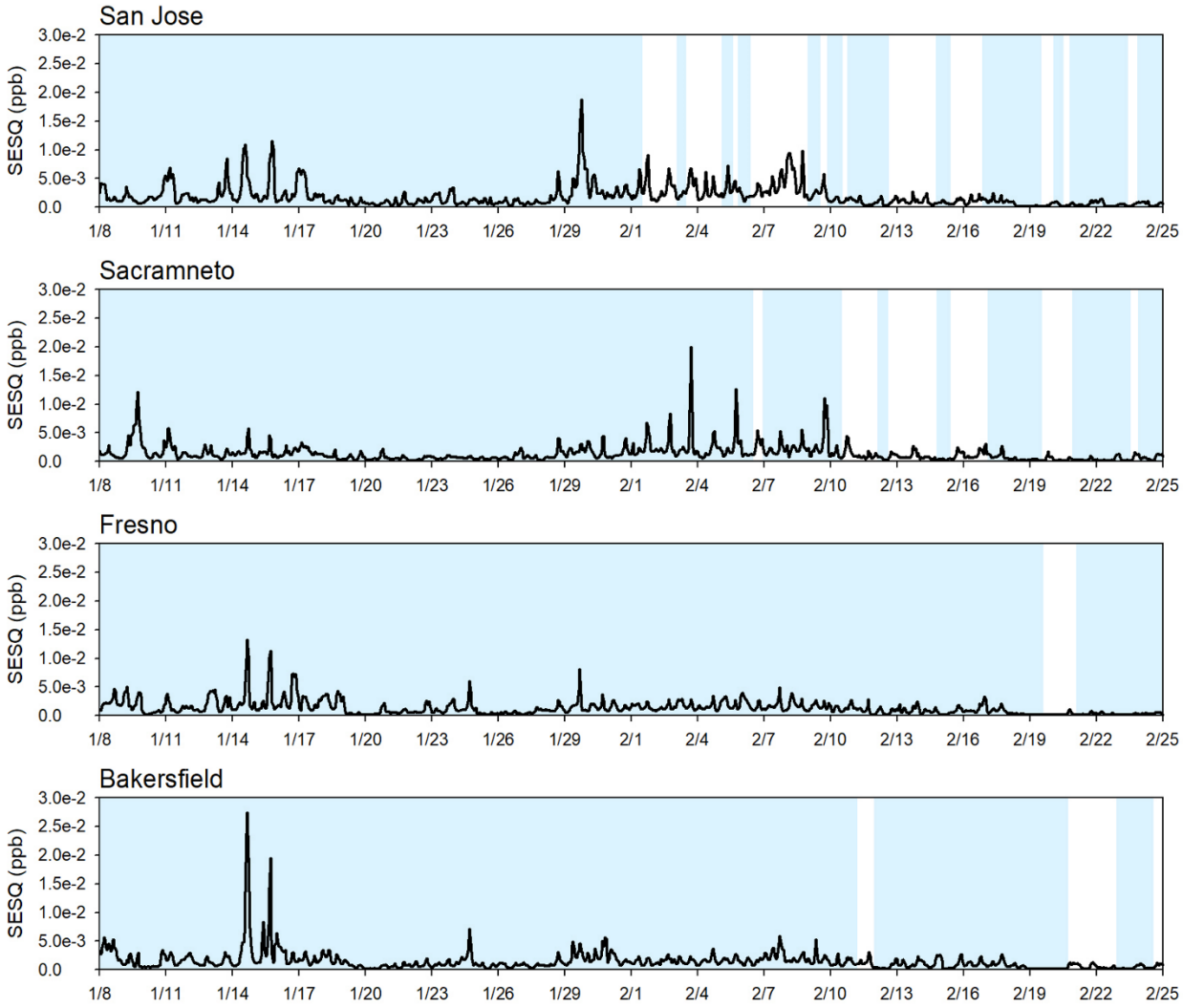

Fig. S8. (Continued)

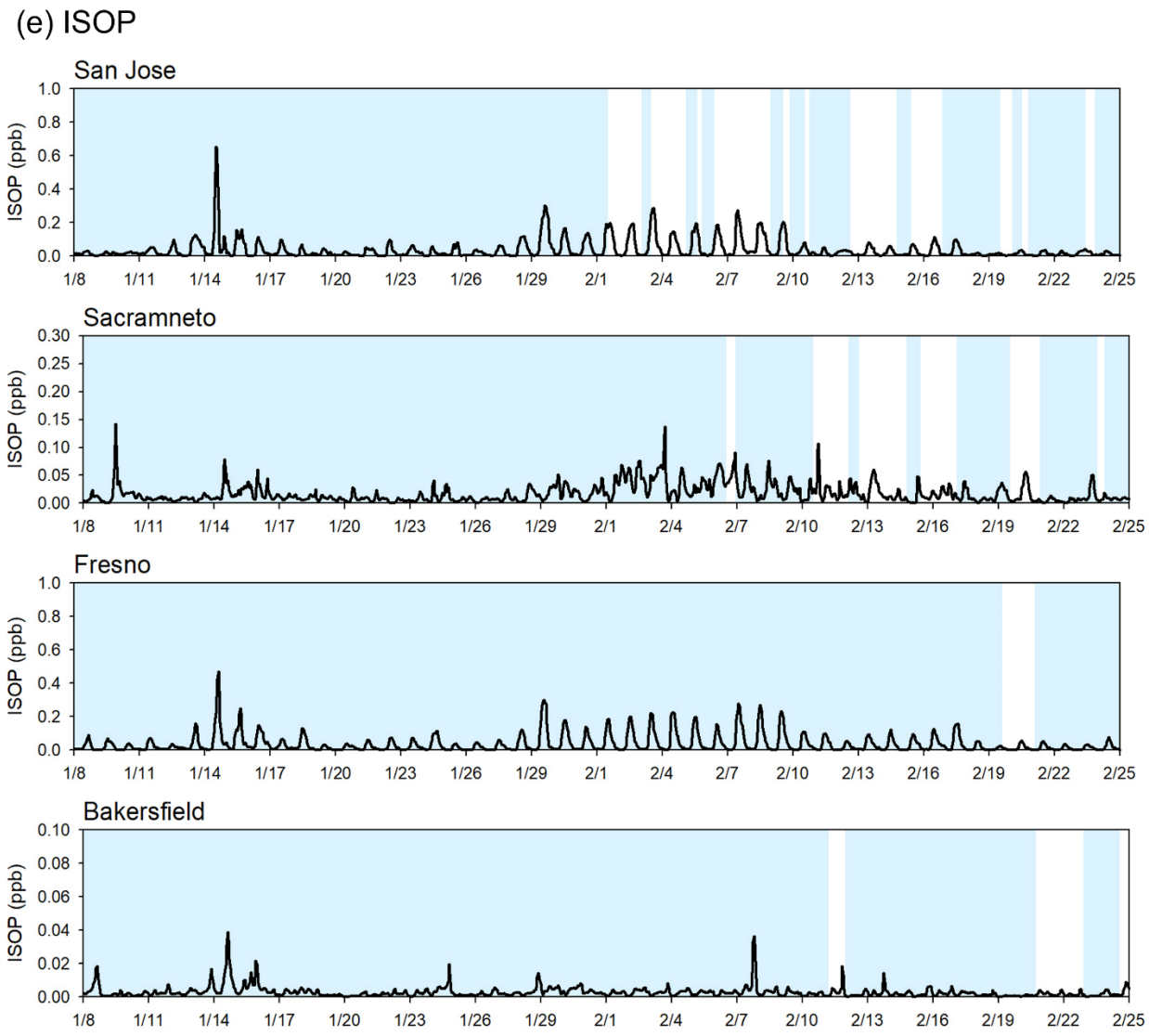

Fig. S8. (Continued)

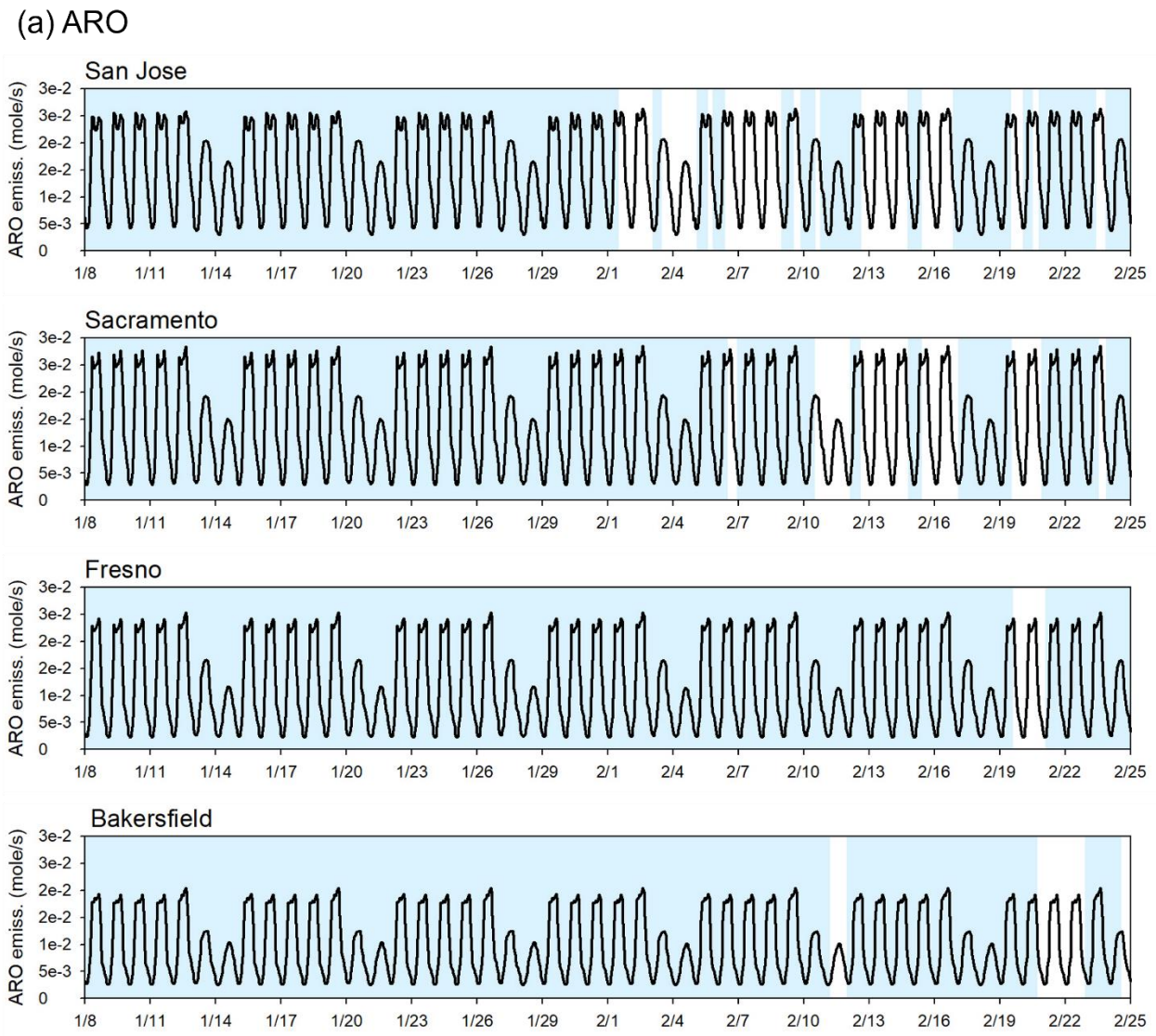

Fig. S9. Time series of emissions of SOA precursor hydrocarbons, (a) ARO, (b) ALK5, (c) TERP, (d) SESQ, and (e) ISOP at each site between January and February in 2018. ARO is the sum of benzene, toluene, o-xylene, p-xylene, m-xylene, and 1,2,4-trimethylbenzene.

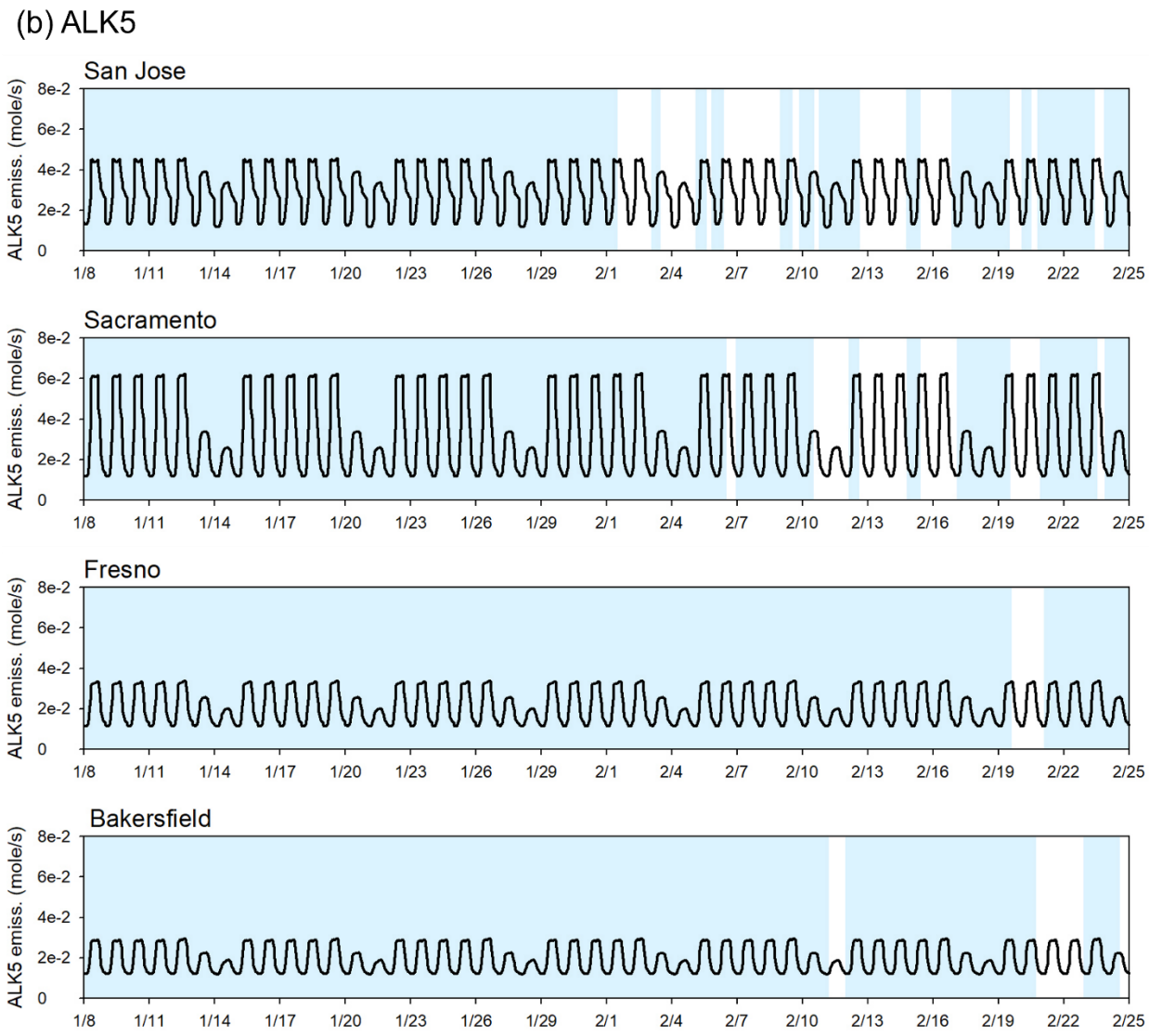

Fig. S9. (Continued)

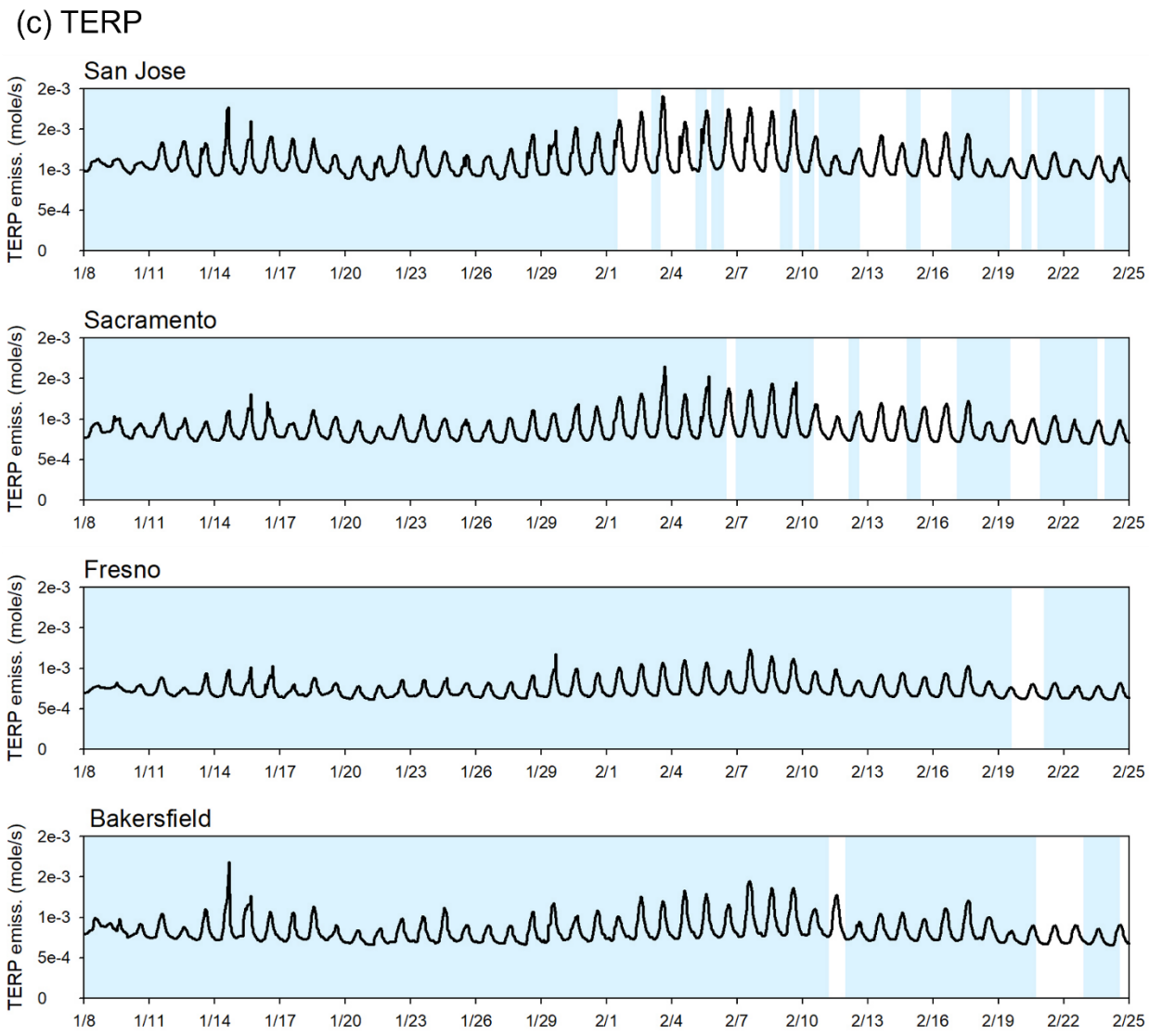

Fig. S9. (Continued)

(d) SESQ

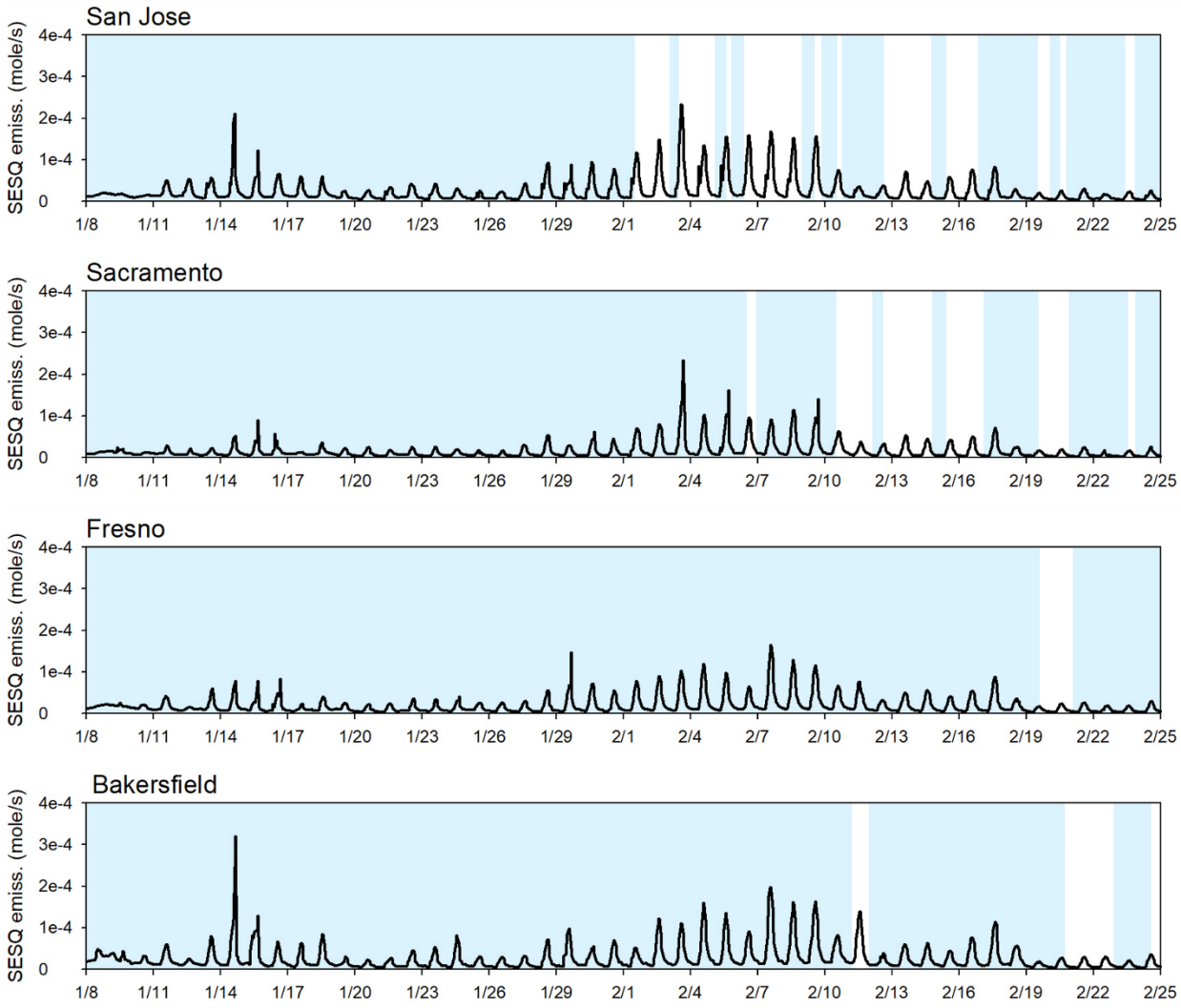

Fig. S9. (Continued)

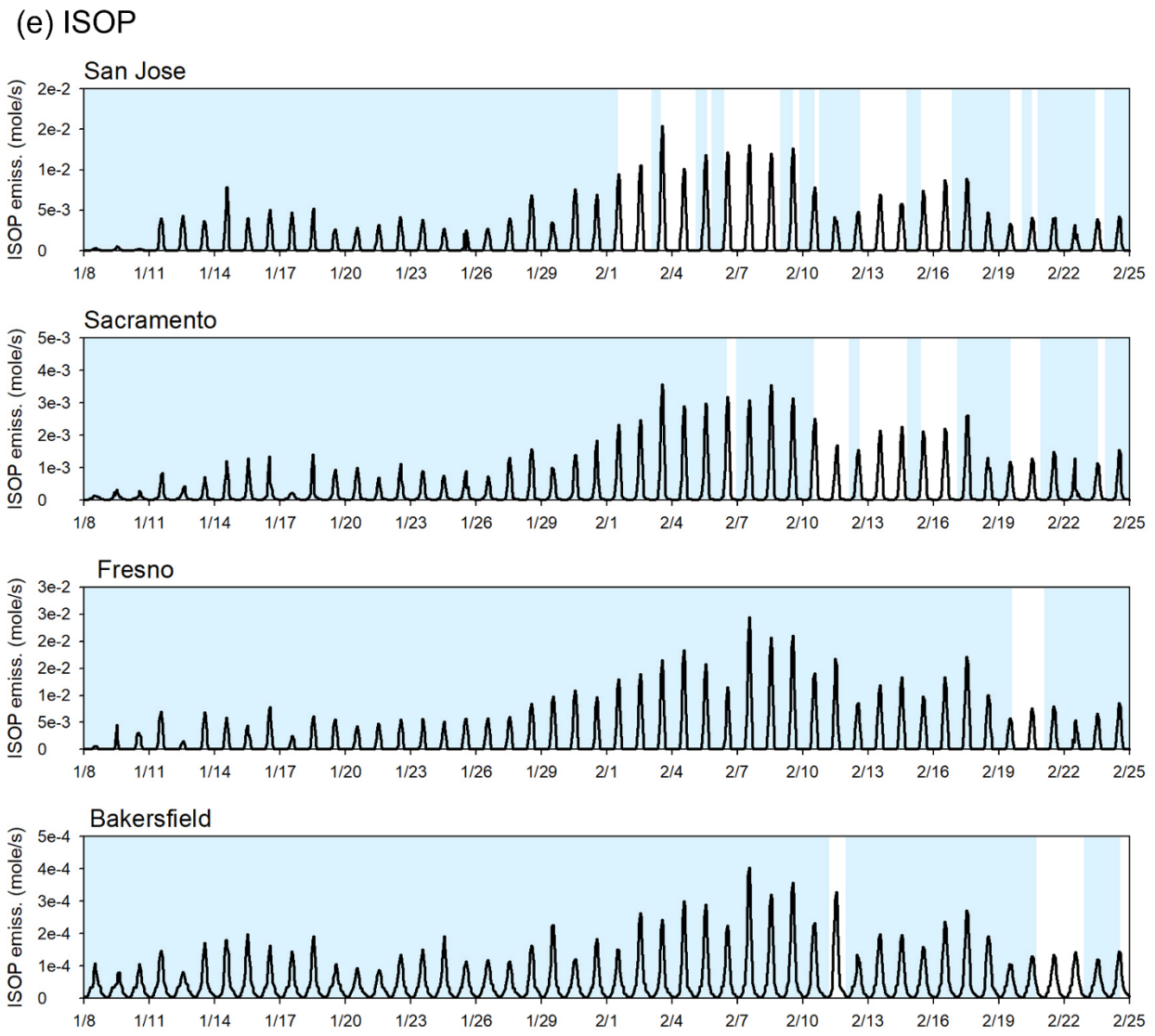

Fig. S9. (Continued)

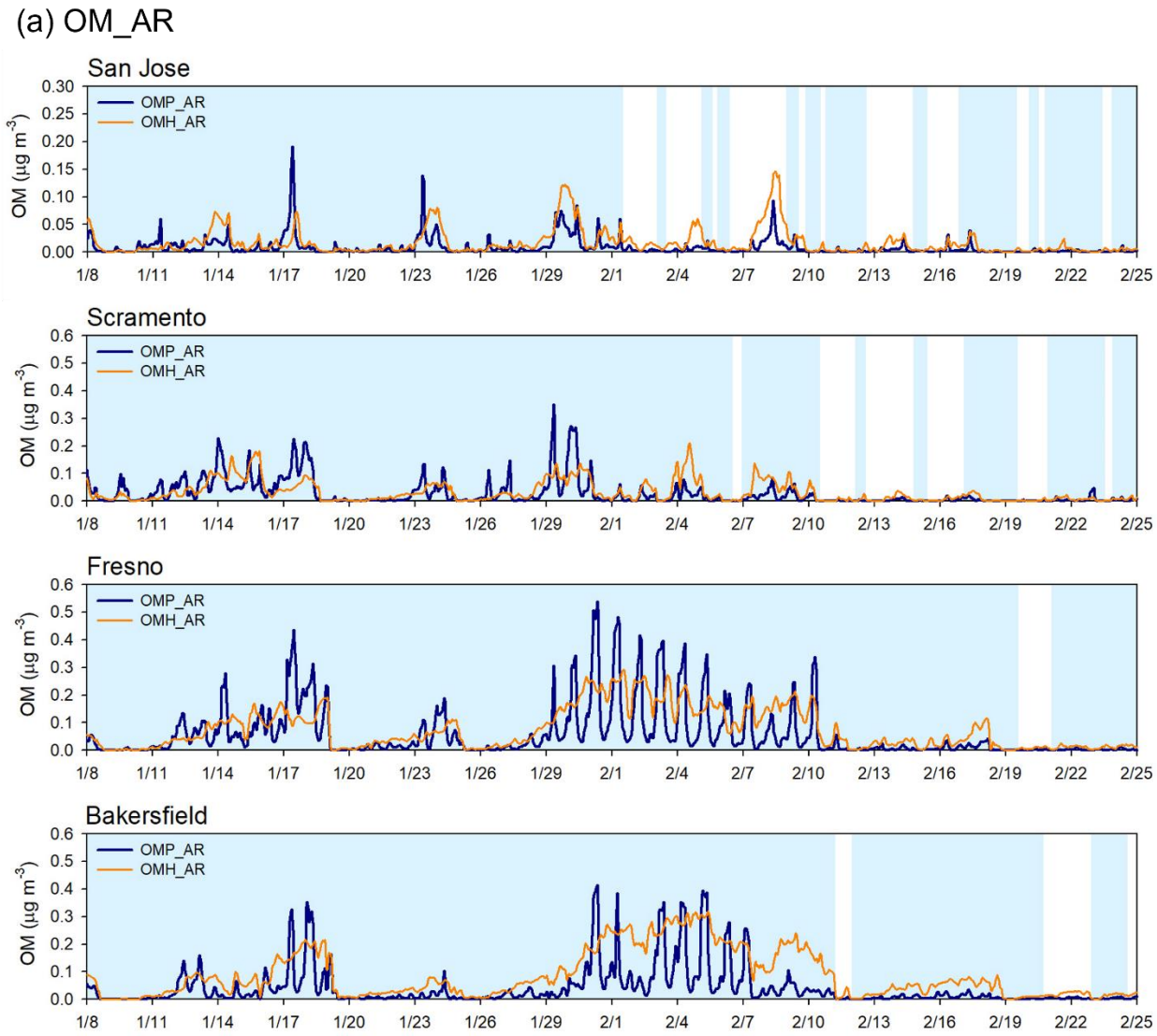

Fig. S10. Time series of hourly simulated SOA species in the UNIPAR model, (a) aromatic SOA, (b) alkane SOA, (c) terpene SOA, (d) sesquiterpene SOA, and (e) isoprene SOA at each site between January and February in 2018. The navy-blue line represents the partitioned SOA (OMP) and orange line represents the heterogeneously formed SOA (OMH).

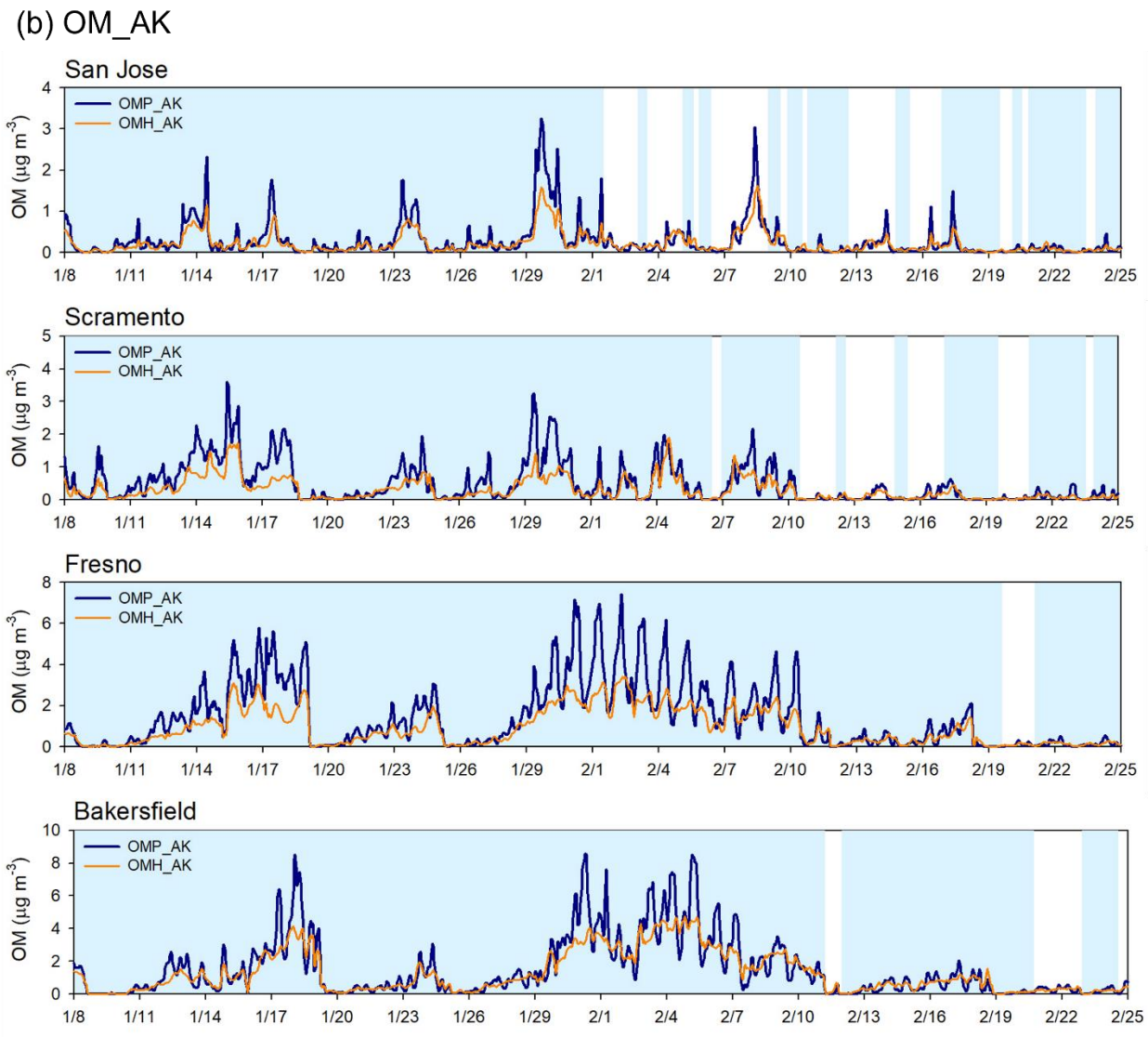

Fig. S10. (Continued)

(c) OM_TE

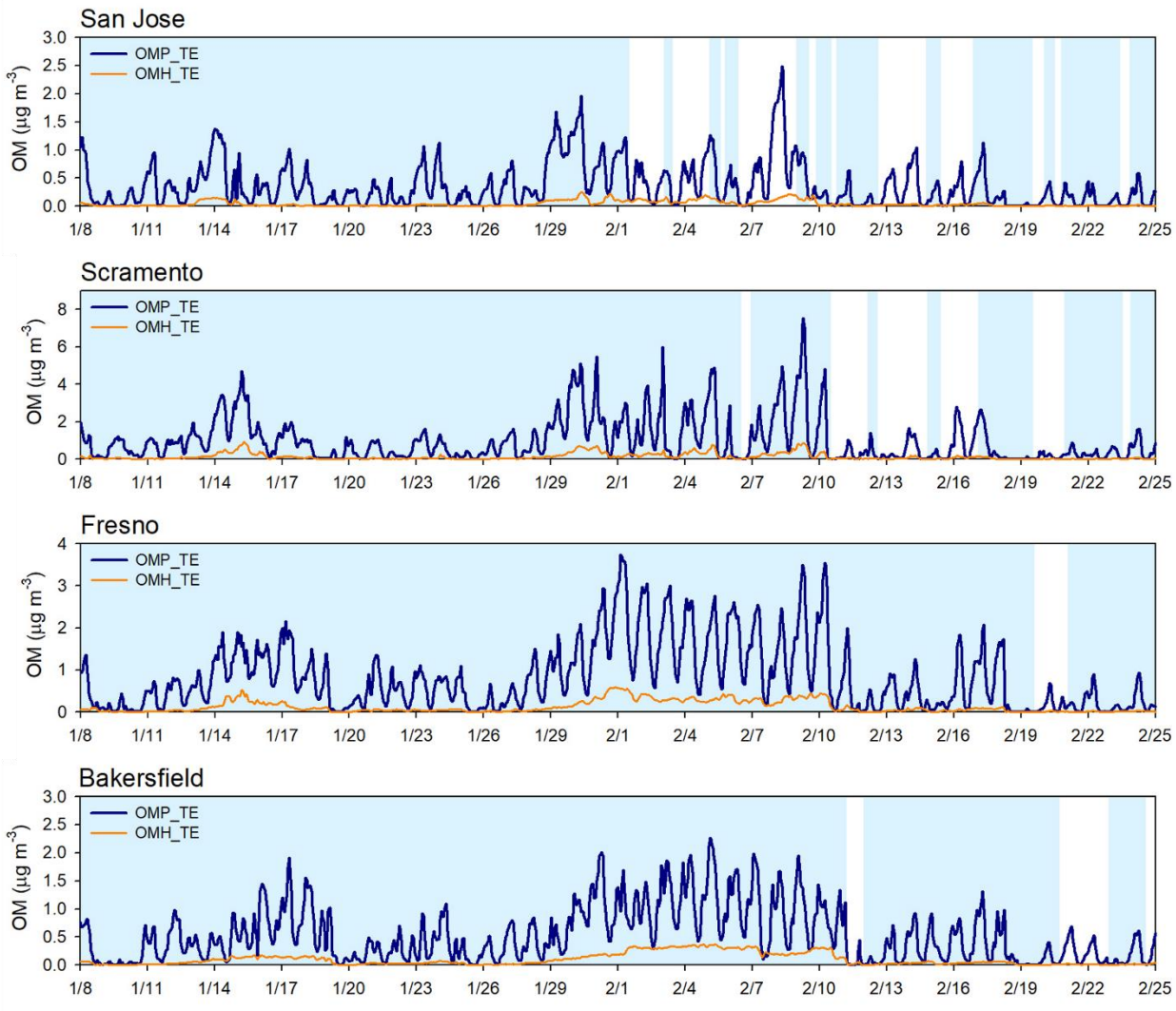

Fig. S10. (Continued)

(d) OM_SP

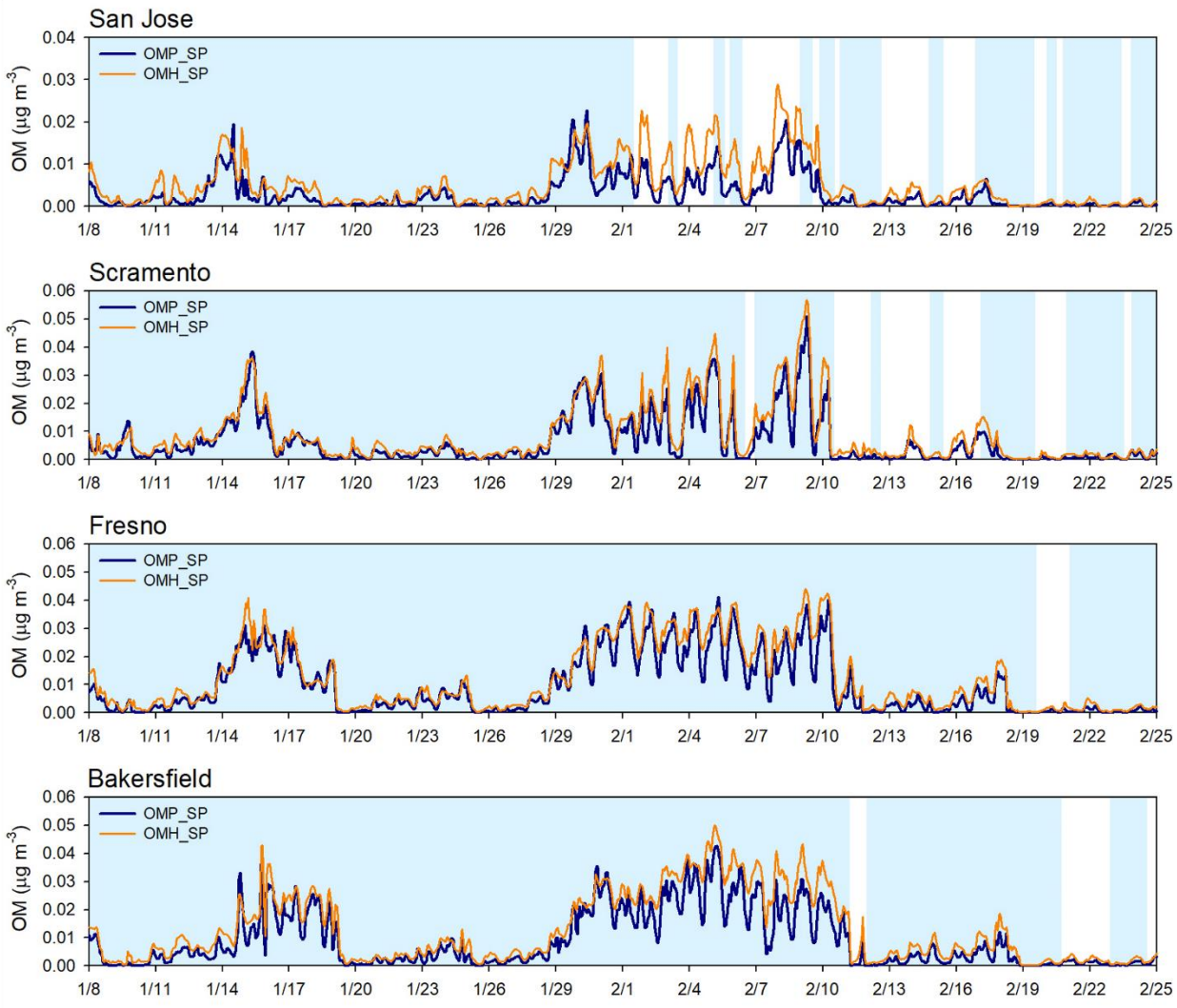

Fig. S10. (Continued)

(e) OM_IS

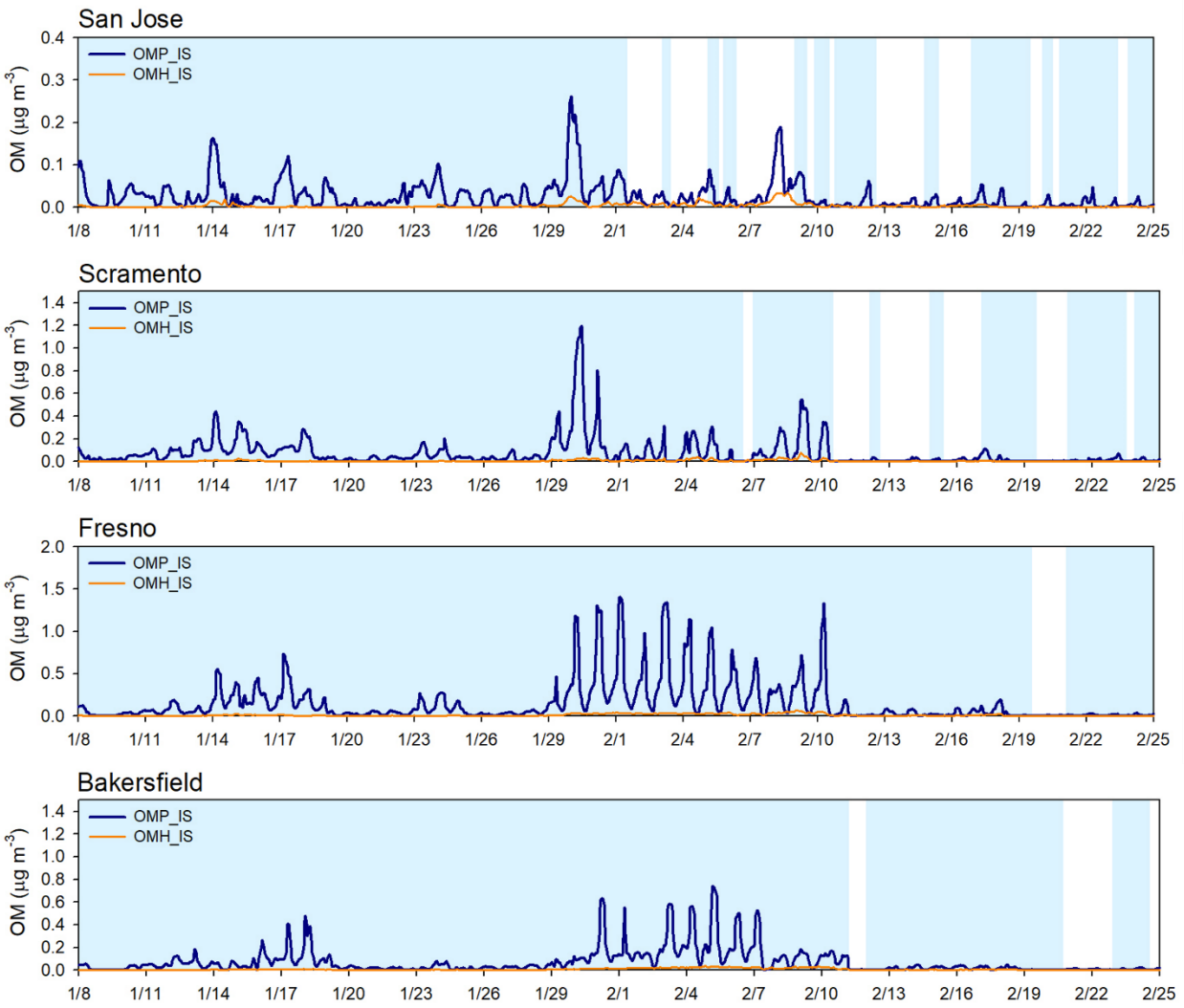

Fig. S10. (Continued)

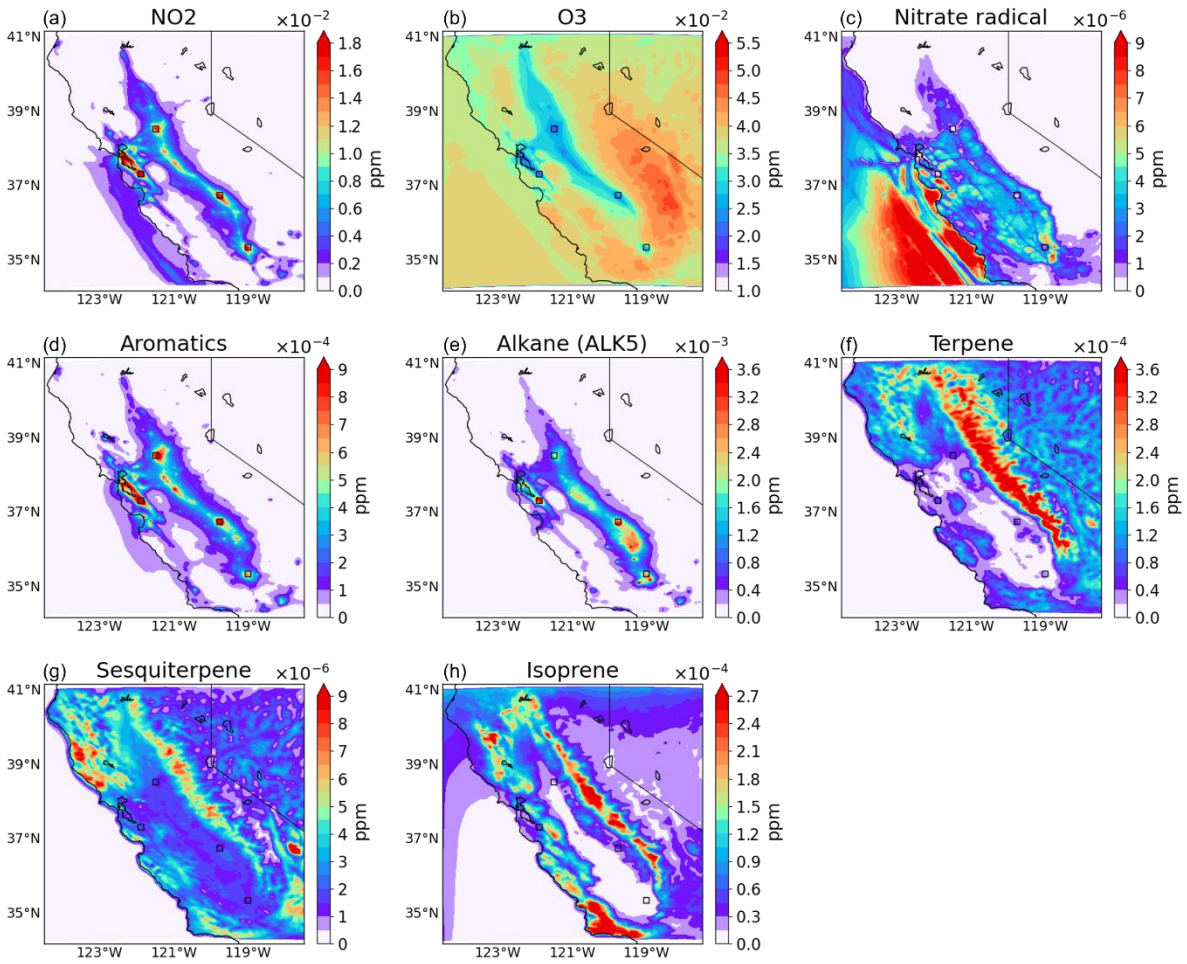

Fig. S11. Spatial distributions of (a) NO_2, (b) Ozone, (c) Nitrate radical, (d) Aromatics, (e) Alkane (ALK5), (f) Terpene, (g) Sesquiterpene, and (h) Isoprene concentrations averaged between 01/23/2018 and 02/24/2018. Aromatics is the sum of benzene, toluene, o-xylene, p-xylene, m-xylene, and 1,2,4-trimethylbenzene.

Section S5. The time series of the predicted concentrations of inorganic species (sulfate, nitrate, and ammonium) and the comparison of aerosol acidity (proton concentration) between the prediction (ISORROPIA model) and observation.

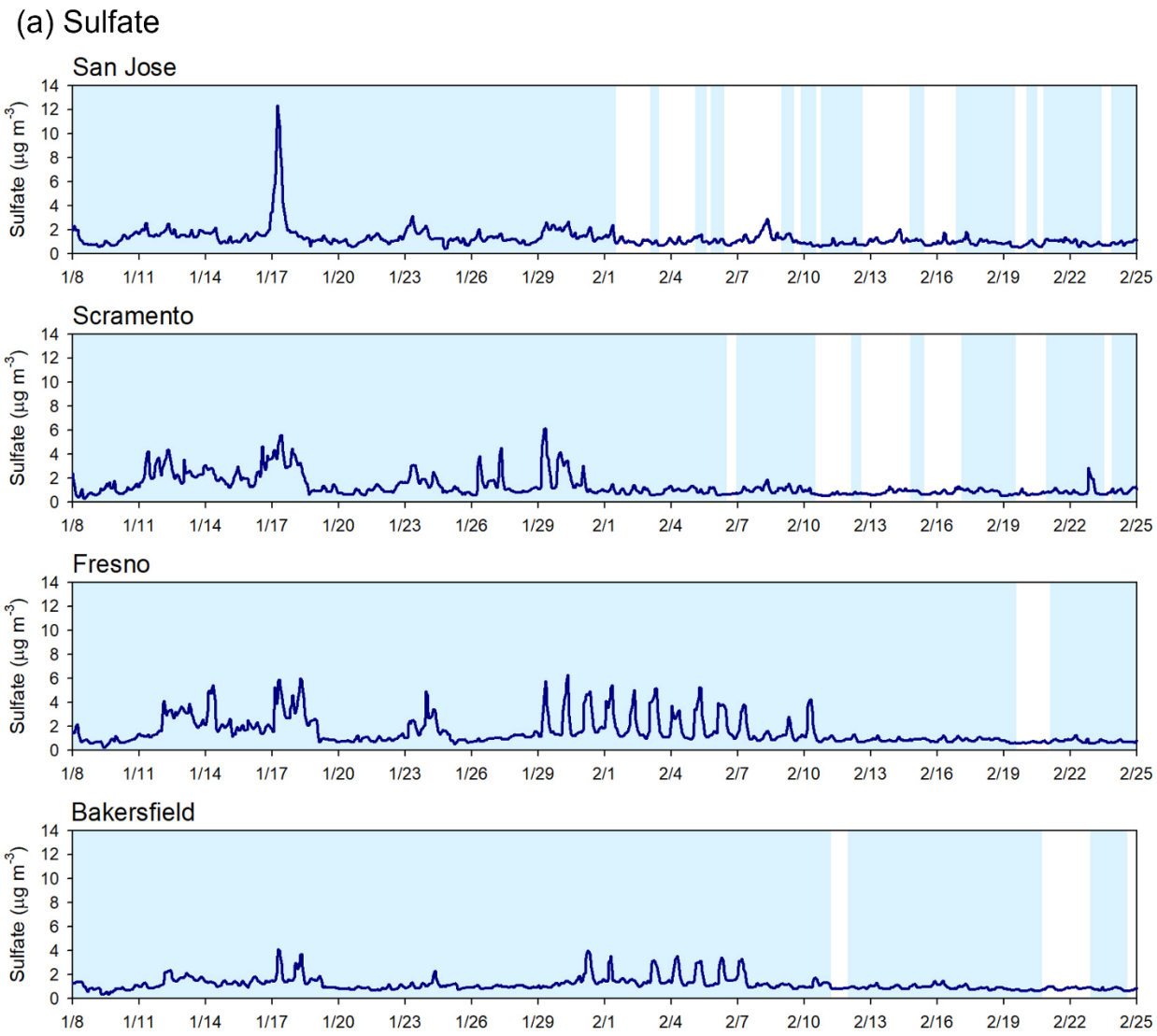

Fig. S12. Time series of hourly simulated (a) Sulfate, (b) Nitrate, and (c) Ammonium at each site between January and February in 2018.

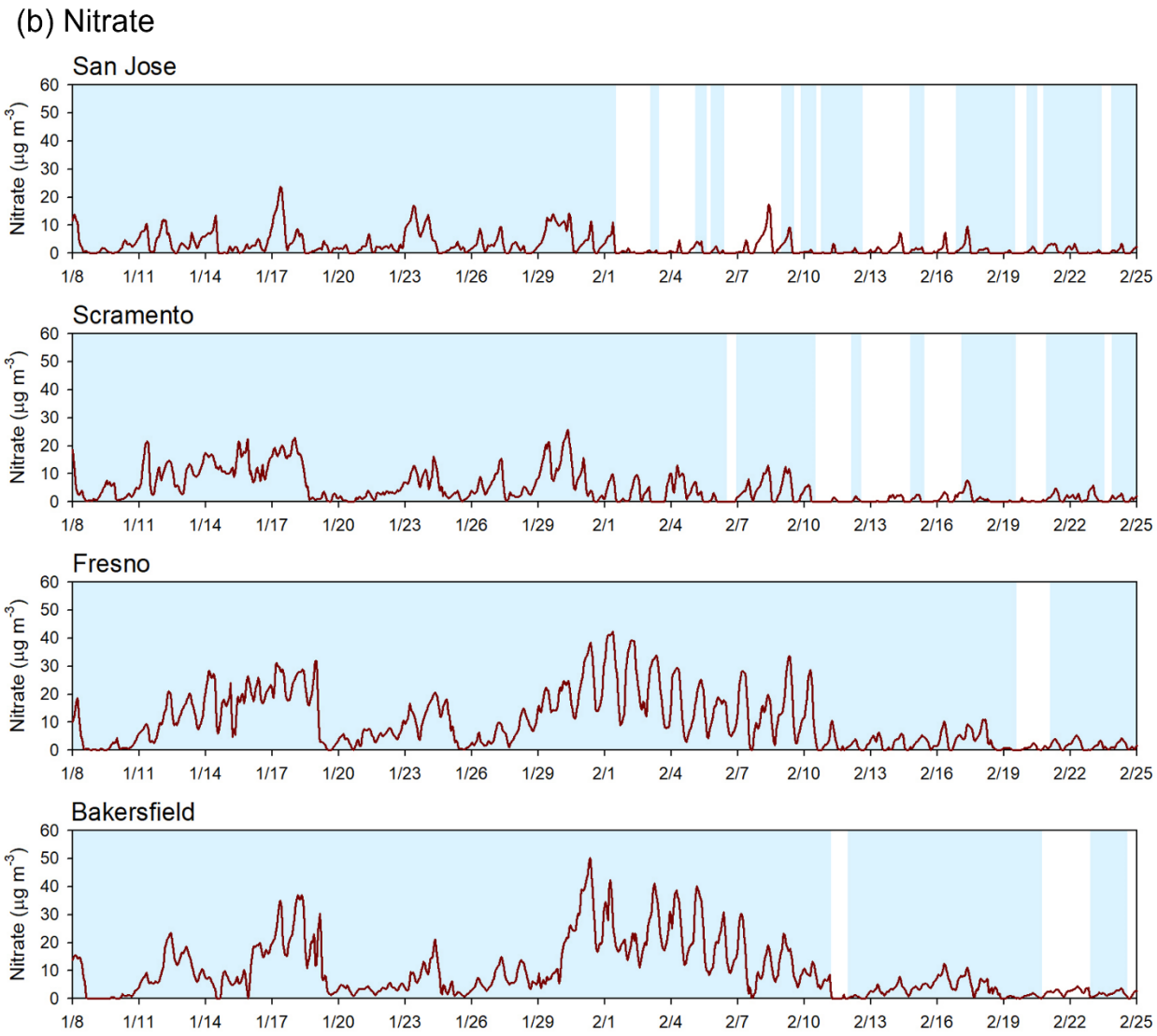

Fig. S12. (Continued)

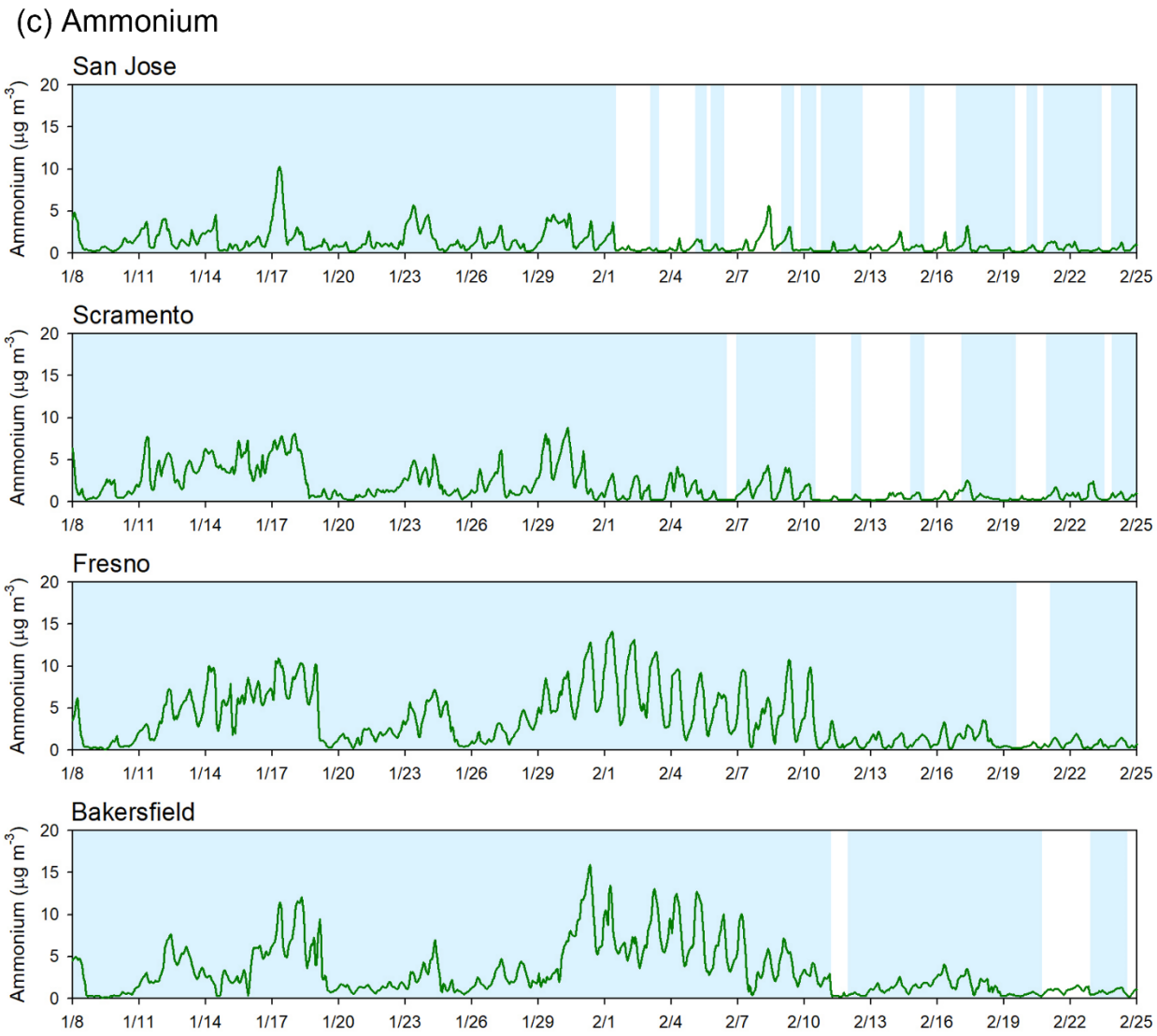

Fig. S12. (Continued)

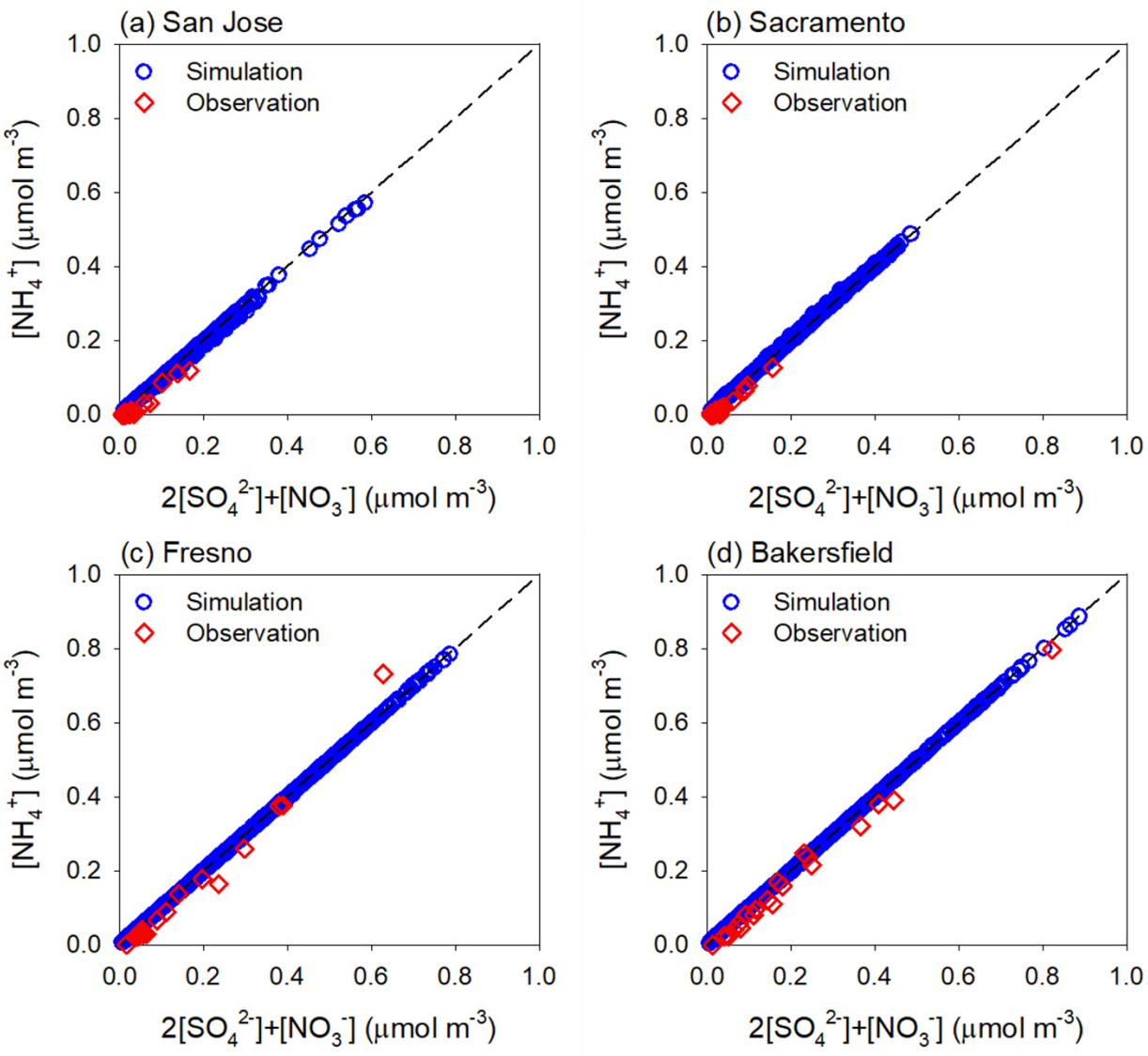

Fig. S13. Scatter plots of observed (red diamond) and simulated (blue circle) anion charges vs. ammonium ions along with the one-to-one line (dash) for the fully titrated inorganic aerosol.

Section S6. The HCHO-to-NO_2 ratio (FNR) in CA and the diurnal variation of simulated PBL height.

FNR < 1 and FNR > 2 correspond to VOC-limited (NO_x-rich) and NO_x-limited conditions, respectively, (Duncan et al., 2010; Hoque et al., 2022).

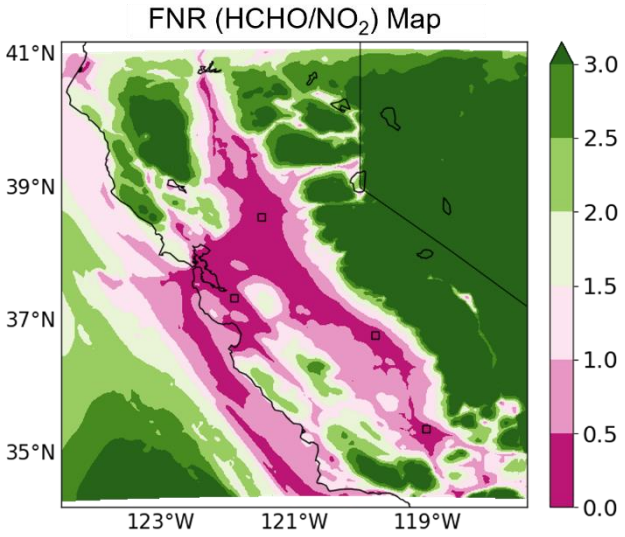

Fig. S14. Spatial distribution of the surface HCHO-to-NO_2 ratio (FNR) from CAMx simulation in CA (February 2018).

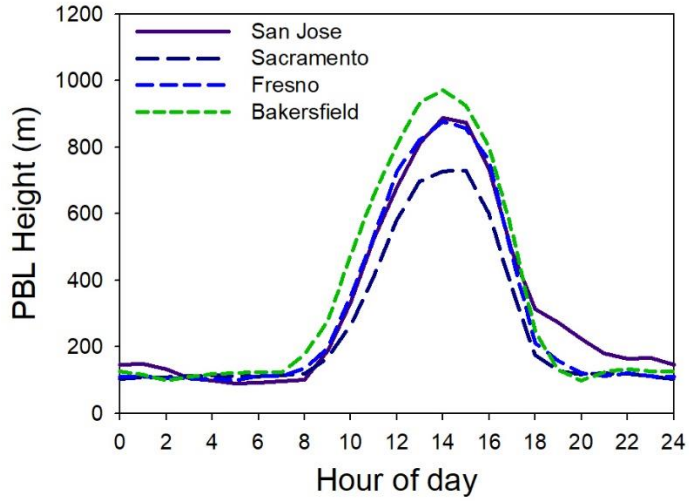

Fig. S15. Diurnal variation of simulated PBL height at four sites averaged between 01/23/2018 and 02/24/2018.

References

Berg, L. K., Gustafson, W. I., Kassianov, E. I., and Deng, L.: Evaluation of a Modified Scheme for Shallow Convection: Implementation of CuP and Case Studies, Monthly Weather Review, 141, 134-147, https://doi.org/10.1175/mwr-d-12-00136.1, 2013.

Colella, P. and Woodward, P. R.: The Piecewise Parabolic Method (PPM) for Gasdynamical Simulations, J. Comp. Phys., 54, 174-201, 1984.

Duncan, B. N., Yoshida, Y., Olson, J. R., Sillman, S., Martin, R. V., Lamsal, L., Hu, Y., Pickering, K. E., Retscher, C., Allen, D. J., and Crawford, J. H.: Application of OMI observations to a space-based indicator of NOx and VOC controls on surface ozone formation, Atmos. Environ., 44, 2213-2223, 10.1016/j.atmosenv.2010.03.010, 2010.

Fountoukis, C. and Nenes, A.: ISORROPIA II: a computationally efficient thermodynamic equilibrium model for K^+-Ca^{2+}-Mg^{2+}-NH^{4+}-Na^+-SO_4^{2-}-NO_3^--Cl^--H_2O aerosols, Atmos. Chem. Phys., 7, 4639-4659, https://doi.org/10.5194/acp-7-4639-2007, 2007.

Hoque, H. M. S., Sudo, K., Irie, H., Damiani, A., Naja, M., and Fatmi, A. M.: Multi-axis differential optical absorption spectroscopy (MAX-DOAS) observations of formaldehyde and nitrogen dioxide at three sites in Asia and comparison with the global chemistry transport model CHASER, Atmos. Chem. Phys., 22, 12559-12589, 10.5194/acp-22-12559-2022, 2022.

Hutzell, W. T., Luecken, D. J., Appel, K. W., and Carter, W. P. L.: Interpreting predictions from the SAPRC07 mechanism based on regional and continental simulations, Atmospheric Environment, 46, 417-429, https://doi.org/10.1016/j.atmosenv.2011.09.030, 2012.

Iacono, M. J., Delamere, J. S., Mlawer, E. J., Shephard, M. W., Clough, S. A., and Collins, W. D.: Radiative forcing by long-lived greenhouse gases: Calculations with the AER radiative transfer models, Journal of Geophysical Research, 113, https://doi.org/10.1029/2008jd009944, 2008.

Jiménez, P. A., Dudhia, J., González-Rouco, J. F., Navarro, J., Montávez, J. P., and García-Bustamante, E.: A Revised Scheme for the WRF Surface Layer Formulation, Monthly Weather Review, 140, 898-918, https://doi.org/10.1175/mwr-d-11-00056.1, 2012.

Morrison, H., Thompson, G., and Tatarskii, V.: Impact of Cloud Microphysics on the Development of Trailing Stratiform Precipitation in a Simulated Squall Line: Comparison of One- and Two-Moment Schemes, Monthly Weather Review, 137, 991-1007, https://doi.org/10.1175/2008mwr2556.1, 2009.

Nenes, A., C. , Pilinis, and Pandis, S. N.: ISORROPIA: A New Thermodynamic Model for Multiphase Multicomponent Inorganic Aerosols, Aquatic Geochemistry, 4, 123-152, 1998.

Pleim, J. E.: A Combined Local and Nonlocal Closure Model for the Atmospheric Boundary Layer. Part I: Model Description and Testing, Journal of Applied Meteorology and Climatology, 46, 1383-1395, https://doi.org/10.1175/jam2539.1, 2007.

Pleim, J. E. and Gilliam, R.: An Indirect Data Assimilation Scheme for Deep Soil Temperature in the Pleim–Xiu Land Surface Model, Journal of Applied Meteorology and Climatology, 48, 1362-1376, https://doi.org/10.1175/2009jamc2053.1, 2009.

Seinfeld, J. H. and Pandis, S. N.: Atmospheric Chemistry and Physics from air pollution to climate change, New York. John Wiley and Sons, Incorporated, 1998.

Willmott, C. J.: On the Evaluation of Model Performance in Physical Geography, in: Spatial Statistics and Models, edited by: Gaile, G. L., and Willmott, C. J., Springer Netherlands, Dordrecht, 443-460, https://doi.org/10.1007/978-94-017-3048-8_23, 1984.

Zhang, L., Brook, J. R., and Vet, R.: A revised parameterization for gaseous dry deposition in air-quality models, Atmos. Chem. Phys., 3, 2067-2082, https://doi.org/10.5194/acp-3-2067-2003, 2003.